https://doi.org/10.5194/egusphere-2026-4435
Preprint. Discussion started: 7 August 2026

Early to Middle Holocene aridification trend in southeastern Iberia and the termination of the last North African Humid Period revealed by a multi-proxy speleothem record

Fernando Gázquez[1,2], Hubert Vonhof[3], Carlos Pérez-Mejías[4], Andrea Columbu[5], Alena Giesche[6], Hai Cheng[4], Alfredo Martínez-García[3], Brian DiMento[7], Eneko Iriarte[8] and José María Calaforra[1,2]

[1] Department of Biology and Geology, Building CITE IIB, Universidad de Almería, Carretera de Sacramento s.n, La Cañada de San Urbano, 04120 Almería, Spain

[2] Andalusian Centre for Global Change- Hermelindo Castro (Engloba), Building CITE V, University of Almería, 04120 Almería, Spain

[3] Climate Geochemistry Department, Max Planck Institute for Chemistry, Mainz, Hahn-Meitner-Weg 1, 55128, Germany,

[4] Institute of Global Environmental Change, Xi'an Jiaotong University, Xi'an 710049, China

[5] Department of Earth Sciences, University of Pisa, Via Santa Maria, 53, 56126, Italy.

[6] Department of Earth Sciences, Colby College, Waterville ME 04901, USA

[7] Department of Chemistry, University of Alaska, Anchorage AK 99508, USA

[8] Área de Paleontología, Departamento de Historia, Geografía y Comunicación, Facultad de Humanidades y Comunicación, Universidad de Burgos, 09001, Burgos, Spain

Correspondence to: Fernando Gázquez (f.gazquez@ual.es)

Abstract. During the Early Holocene, relatively humid conditions prevailed across northern Africa, transitioning to a drier climate by the end of the mid-Holocene. While the timing and nature of this climatic shift are well-established in the Maghreb region of Africa, uncertainties remain regarding the pace of the wet-to-dry transition in the southern Iberian Peninsula. We present a multi-proxy stalagmite record from Simarrón II cave, spanning 9.7 to 4.4 ka BP. The dataset combines stable carbon and oxygen isotopes in calcite ($\delta^{18}O_{carb}$, $\delta^{13}C$), Mg/Ca ratios, petrographic observations, fluid inclusion isotopes ($\delta^{18}O_{fi}$, $\delta^{2}H$) and TEX_{86}-derived paleotemperatures to reconstruct paleohydrological and climatic changes. From 9.7 to 4.4 ka, progressively higher $\delta^{18}O_{fi}$ and $\delta^{2}H$ values, coupled with decreasing deuterium excess, are consistent with a gradual shift in rainfall seasonality and/or moisture sources (i.e., frontal Atlantic-type precipitation regime during the early Holocene to a more convective Mediterranean regime). This trend could be overprinted by enhanced soil and in-cave water evaporation during the late Mid-Holocene because of climate aridification. Lower $\delta^{18}O_{carb}$, $\delta^{13}C$, and Mg/Ca values between 9.7 and 6.0 ka also indicate relatively wet conditions during the early Holocene and part of the middle Holocene. From ~6.0 ka onward, these proxies show a progressive increase, stabilizing after ~5.5 ka, consistent with a climate shift toward more arid conditions that occurred within ~500 yrs. This is interpreted as reflecting enhanced prior calcite precipitation rates and kinetic isotope effects associated with intensified in-cave CO_2 degassing, due to the dry climate during the termination of the last North African

https://doi.org/10.5194/egusphere-2026-4435
Preprint. Discussion started: 7 August 2026

Humid Period. Paired $\delta^{18}O_{carb}$– $\delta^{18}O_{fi}$ paleotemperature estimates yield unrealistically high values (20–30°C) for most of the investigated period, further supporting non-equilibrium fractionation processes and likely in-cave water evaporation. In contrast, TEX_{86}-based temperatures (13–17°C) suggest that early–mid Holocene cave temperatures were higher than present-day values in the cave (11.7°C).

1. Introduction

Despite being the driest region in Europe today, multiple paleoclimate records suggest that the southeastern Iberian Peninsula experienced significantly wetter conditions during the early and part of the mid-Holocene (Jiménez-Moreno and Anderson, 2012; Ramos-Román et al., 2018; Schröder et al., 2018; Toney et al., 2020; García-Alix et., 2022). Indeed, the western Mediterranean region underwent warm and humid conditions during this period, coinciding with the peak of the last North African Humid Period (nAHP) and the associated Sahara greening event (de Menocal et al., 2000). The primary evidence for this humid phase in northwestern Africa is derived from lake sediment cores in the Maghreb (Zielhofer et al., 2017; Cheddadi et al., 2021; Yacoub et al., 2023) and speleothem records from Moroccan caves (Wassenburg et al., 2016; Ait Brahim et al., 2019; Sha et al., 2019). Lacustrine records from both high- and low-elevation sites in the Andalusia region, in southern Spain (Jiménez-Moreno and Anderson, 2012; Ramos-Román et al., 2018; Schröder et al., 2018; Toney et al., 2020; García-Alix et., 2022) further confirm that wetter conditions prevailed across this region between ca. 9 and 6 ka. This pattern is also reflected in the limited speleothem records published to date from caves located near sea level in SE Spain (i.e., the Cueva Victoria speleothem record; 40 m a.s.l.; Budsky et al., 2019). Nevertheless, no speleothem records from higher-altitude sites in SE Iberia are currently available that span the peak of Holocene humidity and the subsequent transition to drier conditions during the late middle Holocene.

Compared to other archives, such as marine or lake sediments, speleothems typically provide higher-temporal resolution records and more precise chronological control (Fairchild et al., 2006). Moreover, the development of new analytical techniques in recent decades is enabling the acquisition of quantitative isotope proxies from cave deposits, which is highly valuable for validating isotope-enabled climate change models (Comas-Bru et al., 2019). These techniques include the analysis of stable isotopes, not only in the carbonate of speleothems ($\delta^{18}O_{carb}$ and $\delta^{13}C$) but also in fluid inclusions trapped within their structure ($\delta^{18}O_{fi}$ and $\delta^{2}H$). Since the incorporation of water into these fluid inclusions is not affected by stable isotope fractionation during mineral precipitation, such analyses provide direct information on the isotopic composition of drip water in the cave and, consequently, on changes in rainfall patterns and/or shifts in the moisture source affecting the cave site, among other hydroclimate processes (see Affolter et al., 2025 for a review). In some cases, by combining $\delta^{18}O_{carb}$ and $\delta^{18}O_{fi}$, it is possible to calculate paleotemperatures (Genty et al., 2002; Griffiths et al., 2010; Demény et al. 2021; Bernal-Wormull et al., 2025). In addition, paleothermometers based on the chemistry of organic compounds trapped in speleothems have also been developed, such as the TEX86 paleothermometer, which relies on the relative abundance of Glycerol Dialkyl Glycerol

Tetraethers (GDGTs) preserved in speleothem calcite (Blyth and Schouten, 2013; Baker et al., 2019; Wassenburg et al., 2021; Levy et al., 2023).

In this study, we investigate a stalagmite (SM4) from Simarrón II cave (Almería, SE Spain) using a multi-analytical approach. We combine conventional techniques, such as stable oxygen and carbon isotope analysis in carbonates, Mg/Ca ratio measurements, and petrographic studies, which provide insights into the cave's hydrological regime in connection with external climate conditions, with recently developed methods, including stable isotope analysis of fluid inclusions and the TEX86 paleothermometer. The objective is to generate a high-resolution paleohydrological record from an alpine area in the southeastern Iberian Peninsula and to understand how climate changed during the Early and Middle Holocene, including the termination of the last nAHP. Our study sheds light on the climatic mechanisms that triggered this major climate shift in the northern Hemisphere.

2. Geological and climate setting

Simarrón II cave (36º51'01'' N; 2º48'33'' E) is located on the southern flank of the Sierra de Gádor mountain range (Almería Province, SE Spain), in an area known as Pecho Cuchillo, a plateau situated approximately 14 km from the Mediterranean coast (Fig. 1A and B). The cave entrance is at 1493 m a.s.l, and it reaches a maximum depth of 70 m and a total surveyed length of 453 m (Torres, 1994). The stalagmite SM4 investigated in this study was collected from the chamber known as Salas Vías Blancas, located approximately 30 m below the surface (Fig. 1C).

The cave developed within highly fractured Triassic carbonate rocks. These carbonates are interbedded with low-permeability calcschist layers and are underlain by impermeable Permian phyllites. Together, these lithologies form one of the most important karst aquifers in the southeastern Iberian Peninsula (Vallejos et al., 1997; Pulido-Bosch et al., 2000). The geological structure of the Sierra de Gádor has been significantly affected by tensional and strike-slip faulting, which facilitated the formation of caves along fractures, with little or no evidence of chemical dissolution. This is the case for Simarrón II cave and other nearby cavities in this area (Sánchez-Martos et al., 1991). Modern speleothem precipitation is uncommon in such caves due to the limited role of dissolution processes and the present-day arid climate.

https://doi.org/10.5194/egusphere-2026-4435
Preprint. Discussion started: 7 August 2026

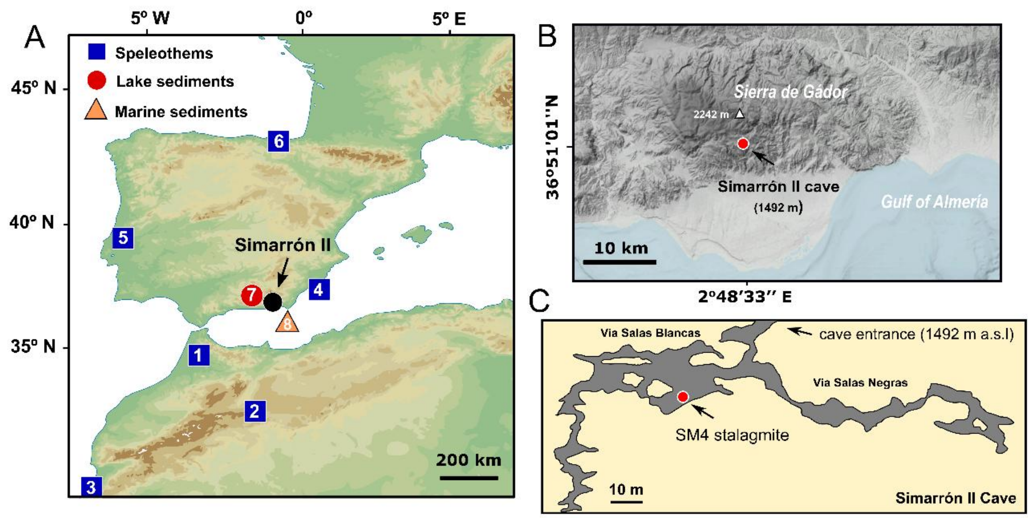

1.

Figure 1. (A) Location of Simarrón II cave in the context of the Iberian Peninsula. The location of the main paleoclimate records used for comparison in this study are indicated: 1. Piste cave (Wassenburg et al., 2016); 2. Chaara cave (Ait Brahim et al., 2019); 3. Wintimdouine cave (Sha et al., 2019); 4. Cueva Victoria cave (Budsky et al., 2019); 5. Buraca Gloriosa cave (Thatcher et al., 2020); 6. Mendukilo cave (Bernal-Wormull et al., 2023); 7. Lakes in Sierra Nevada mountain range, including Laguna de Rio seco (Jiménez-Espejo et al., 2014) and Padul peat bog (Camuera et al., 2022); 8. Marine sediments from the Alboran sea, including sediment cores MD95204 (Cacho et al., 1999) and 293G (Rodrigo-Gámiz et al., 2014). (B) Location of Simarrón II cave in Sierra de Gádor mountain range. (C) Profile of Simarrón II cave (topography by Speleoclub Almería). The location where the SM4 stalagmite was collected is indicated.

The Mediterranean-type climate of the area is characterized by warm, dry summers and mild winters, with most precipitation occurring in late winter and spring. The primary source of moisture in southeaster Iberia is provided by Atlantic frontal systems, which account for most winter-spring precipitation, whereas convective rainfall of local and Mediterranean origin becomes increasingly important during summer (Paredes et al., 2006). Precipitation variability, both under present-day conditions and throughout the past, has been largely controlled by changes in the phase of the North Atlantic Oscillation (NAO) (Toney et al., 2020; Gázquez et al., 2025).

The mean annual precipitation in the Sierra de Gádor is approximately 250 mm (1997–2025 period), although interannual and spatial variability can be significant, with differences of up to 250 mm between the highest and lowest elevations. There is an altitudinal precipitation gradient of 17 mm per 100 m and snow occasionally falls above 1800 m a.s.l. during the winter months

https://doi.org/10.5194/egusphere-2026-4435
Preprint. Discussion started: 7 August 2026

(Vallejos et al., 1997). The mean annual cave temperature in the Salas Vías Blancas Hall of Simarrón II cave, where stalagmite SM4 was collected, was 11.7 °C (2005–2006 period), with minimal annual variation (±0.2 °C) (Mayoral et al., 2022). In-cave relative humidity is attested between 80% and 90% for most of the year, dropping to 65–75% during the summer months (Mayoral et al., 2022).

Vegetation cover above the cave is currently sparse, consisting mainly of shrub and herbaceous species, with dominant taxa from the Asteraceae, Fabaceae, and Brassicaceae families (Giménez-Luque and Gómez-Mercado, 2002). The area corresponds to the thermomediterranean semi-arid vegetation belt, and also includes scattered patches of reforested pine (mainly *Pinus halepensis* and *Pinus nigra*).

3. Materials and Methods

3.1. Stalagmite SM4

Sample SM4 is a fragment of a stalagmite collected from the chamber of Simarrón cave II known as Salas Vías Blancas, located approximately 30 m below the surface. The stalagmite was naturally broken when collected, and neither the apical nor the basal parts are preserved. The investigated fragment is 413 mm long and consists of compact laminated carbonate, with no evidence of recrystallization or dissolution cavities. The stalagmite fragment was cut along its longitudinal axis, and subsamples were extracted using a Dremel tool equipped with different bits depending on the requirements of the analyses.

3.2. Mineralogy and petrography

In order to confirm that the speleothem mineralogy is entirely composed of calcite, X-ray diffraction (XRD) analyses were conducted on six powder samples (~150 mg) extracted from stalagmite SM4 at different depths using a Dremel tool. The analyses used a D8 ADVANCE DAVINCI diffractometer equipped with a copper radiation tube (CuKα, λ = 0.154 nm), a graphite monochromator, and a LYNXEYE XE detector at the Central Research Services of the University of Almería, Spain. The operating voltage and current were set to 40 kV and 30 mA, respectively. Data were collected using the 2θ scan method with a counting time of 0.400 s per step, over an angular range of 5° to 80°. Mineral phases were identified by comparison with the PDF-2 database using XPowder software.

Petrographic observations were conducted on thin sections using a Zeiss AxioZoom V16 operating at the Earth Sciences Department, University of Pisa, Italy (Columbu et al., 2024). Fabrics are described according to Frisia (2015).

https://doi.org/10.5194/egusphere-2026-4435
Preprint. Discussion started: 7 August 2026

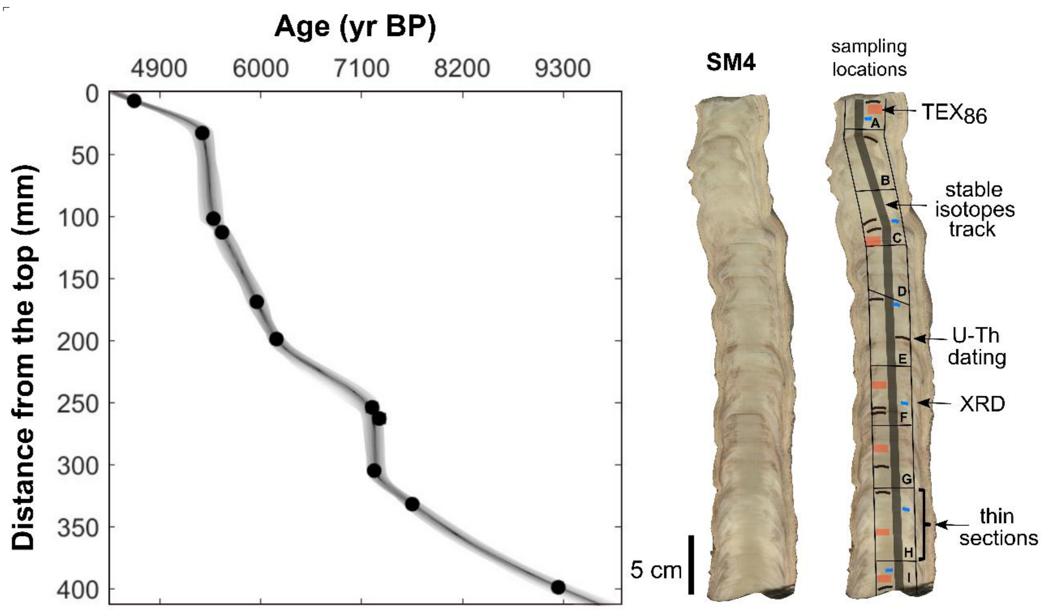

Figure 2. Age model of stalagmite SM4 from Simarrón II cave and sampling location for different analytical techniques applied in this study.

3.3. U-Th dating

U-Th radiometric analyses were performed on eleven powder samples of approximately 100 mg extracted along the main growth axis of SM4 (Fig. 2 and Supplements), with a spatial resolution of 2-3 mm. The sampling targeted areas characterized by dense, pure carbonate with lighter coloration, while avoiding zones with darker colors that may have higher detrital content. The samples were dated at Xi'an Jiaotong University (China) using the uranium-series (U–Th) dating method, following Cheng et al. (2000). Analyses were carried out using a multicollector inductively coupled plasma mass spectrometer (MC-ICP-MS; Thermo-Finnigan™ Neptune) using decay constants reported in Cheng et al., (2013). An age–depth model for the stalagmite was subsequently constructed using the COPRA algorithm implemented in MATLAB (Breitenbach et al., 2012).

3.4. Oxygen and carbon stable isotopes in carbonate

A total of 434 samples (~200 µg each) for $\delta^{18}O$ and $\delta^{13}C$ analyses were collected along the central growth axis of stalagmite SM4 using a Dremel tool at 1 mm intervals, except for the section between 323 and 343 mm from the top, where higher-resolution sampling at 0.5 mm intervals was applied (Fig. 2). Isotopic analyses were performed in the IsoTOPIK Lab at the University of Burgos, Spain, using a ThermoFisher Delta V Plus isotope ratio mass spectrometer coupled to a GasBench II, following the methodology described by Spötl (2011). Long-term analytical reproducibility (1σ) was ±0.06‰ for $\delta^{18}O$ and ±0.08‰ for $\delta^{13}C$.

https://doi.org/10.5194/egusphere-2026-4435
Preprint. Discussion started: 7 August 2026

The same analyses were conducted in the carbonate leftovers after crushing for fluid inclusion measurements (5 mm resolution, see section 3.5), in order to directly compare carbonate and fluid inclusions isotopes within the same samples. In this case, $\delta^{18}O$ and $\delta^{13}C$ analyses were conducted at Inorganic Gas Isotope Geochemistry laboratory at the Max-Planck Institute for Chemistry, Mainz, Germany using also a ThermoFisher Delta V Plus isotope ratio mass spectrometer coupled to a GasBench II. Long-term analytical reproducibility (1σ) was better than 0.1‰ for $\delta^{18}O$ and $\delta^{13}C$. All isotope values are reported in per mil (‰) relative to the Vienna Pee Dee Belemnite (VPDB) standard.

3.5. Stable isotopes in fluid inclusions

Speleothem fluid inclusion water isotopes were measured at the Inorganic Gas Isotope Geochemistry laboratory at the Max-Planck Institute for Chemistry, Mainz, Germany. Eighty-six calcite chips (0.07–0.27 g) were cut using a Dremel Microdrill equipped with a 38 mm diameter diamond-covered circular saw along the growth axis with a 5 mm resolution (Fig. 2). Additional material from five depths was collected to evaluate reproducibility of the analyses. Fluid inclusion water stable isotopes were measured using a humidified (H_2O) nitrogen (N_2) carrier gas line at 110 °C, connected via a crusher unit to a Picarro L2140i cavity ring-down spectrometer (CRDS) where H_2O concentrations, δ^2H and $\delta^{18}O$ were continuously measured (de Graaf et al., 2020). The system was shown to have insignificant memory effect and minimal long-term instrumental drift. Speleothem chips were crushed in a stainless-steel crusher unit with two Teflon coated Viton O-Rings which released fluid inclusion water directly mixed into the humidified carrier gas line for subsequent isotope analysis. Further details of the data processing methods and calibration can be found in de Graaf et al., (2020). Results are given in per mil units (‰) vs. VSMOW. Based on the duplicate analysis (1SD) of the calcite chips collected at five depths, mean reproducibility was 0.1‰ for $\delta^{18}O$, 0.5 ‰ for δ^2H and 0.8‰ for d-excess.

3.6. Mg/Ca ratio

Sampling for Mg/Ca analyses used the same track as for stable isotope analyses. However, sampling resolution was set at 10 mm and a total of 41 powder samples were collected using a Dremel tool (Fig. 2). Samples were dissolved in trace metal grade 3% HNO_3 and diluted to an approximate concentration of 1 ppm Ca. Samples were analyzed at Colby College, Waterville ME, USA using a Spectro ARCOS FHE12 inductively coupled plasma optical emission spectrometer (ICP-OES). Quality control check standards (n=6) for Ca and Mg averaged 99.2 ± 0.8% accuracy. Each sample was analyzed in triplicate with an average relative standard deviation (RSD) of 0.96% for Ca and Mg.

3.7. GDGTs (TEX_{86}) analyses

Glycerol dialkyl glycerol tetraethers (GDGTs) in speleothem SM4 were analyzed at the Organic Isotope Geochemistry Laboratory, Max Planck Institute for Chemistry, Mainz, Germany. Six speleothem chips (approximately 20 × 20 mm, weighing between 0.92 and 1.41 g) were cut along the main growth axis at different distances from the base (Fig. 2) using a Dremel

https://doi.org/10.5194/egusphere-2026-4435
Preprint. Discussion started: 7 August 2026

Microdrill equipped with a 38 mm diameter diamond-coated circular saw. The powdered samples were placed in a 60 mL cylindrical glass vial before being digested in 5-7 mL (~5 mL per gram of sample) of 6 M HCl on a heating plate at 100 °C for 2 h. The dissolved samples were then cooled to room temperature and extracted in a separation funnel using 3×20 mL dichloromethane (DCM). The bottom organic-DCM phases were carefully collected in 60 ml vials, and 40 µL of C46 internal standard was added to the extracts. Extracts were evaporated and dried in an Automated Evaporation System (Rocket Evaporator), followed by re-dissolution in a DCM–methanol mixture. Traces of acid and other impurities were removed by passing solutions through a 5% deactivated silica column and collected in 4 mL vials. The eluates were dried and filtered with a 0.2 µm PTFE membrane filter by rinsing with a 1.8% mixture of isopropanol in n-hexane. Measurements of the extracts were done using an Agilent 1260 Infinity high-performance liquid chromatography (HPLC) unit coupled to an Agilent 6130 single-quadrupole MS. GDGT signals for the isoprenoid GDGT compounds (GDGT-0, GDGT-1, GDGT-2, GDGT-3, crenarchaeol, crenarchaeol isomer (Cren’)) and GDGT C46 were integrated using the Agilent LC/GC-MS data analysis software Mass Hunter according to their mass-to-charge ratio (m/z). The tetraether index (TEX86) was calculated using the following equation (Eq. 1):

$$TEX_{86} = (GDGT2+GDGT3+Cren')/(GDGT1+GDGT2+GDGT3+Cren')$$

We used the following calibration by Blyth and Schouten (2013) to reconstruct cave temperatures (T_{cave}):

$$T_{cave} = 7.34\ (\pm 2.71) + 34.64\ (\pm 4.16) \times TEX_{86}$$

An in-house standard made of an unnamed flowstone sample, was used as an internal standard for every GDGT analysis batch. This standard was analysed at least in duplicate in each batch of samples analysed, obtaining an average cave *T* of 14.57 °C with a standard deviation of 0.28 °C (1SD, $n = 5$). The calibration uncertainty associated with speleothem TEX_{86} is approximately ±1 °C (2 SD) over the temperature range covered by the samples analyzed in this study. It should be emphasized, however, that this uncertainty primarily influences reconstructed absolute temperatures rather than the relative variability between individual samples.

4. Results

4.1. Mineralogy and petrography

XRD analyses of the six powder samples indicate that speleothem SM4 is composed of calcite, with no evidence of other carbonate phases (e.g., aragonite) or significant detrital minerals (e.g., quartz or clay minerals). Petrographic observations confirm the ubiquity of calcite and the relative absence of pervasive detrital layers. Calcite fabric is mostly columnar microcrystalline, characterized by elongated crystals with irregular crystal boundaries (Fig. Sup. 1). This is typically found in laminated stalagmites due to the abundance of organic colloids and particulates, and confers a milky-opaque color at naked

https://doi.org/10.5194/egusphere-2026-4435
Preprint. Discussion started: 7 August 2026

eye (Frisia, 2015). More regular crystal boundaries could be associated to classical columnar calcite (Fig. Sup. 1), implying a slight reduction in the input of colloids and particulates. Diagenetic features are absent, thus dissolution-recrystallization processes, likely compromising the reliability of U-Th chronology and climate proxies, can be excluded. A potential growth hiatus can be observed at ca. 30 mm from the top (Fig. Sup. 1), so that a minor stratigraphic discontinuity may occur between the ages 4,621±12 and 5,364±38 yr BP (Fig. 2). Although the age model cannot constrain the duration of this potential hiatus, the growth rate in this section reaches very low values (Fig. 3), which could suggest either a temporary suspension of water infiltration into the karst system or infiltration of waters that were poorly saturated with respect to $CaCO_3$.

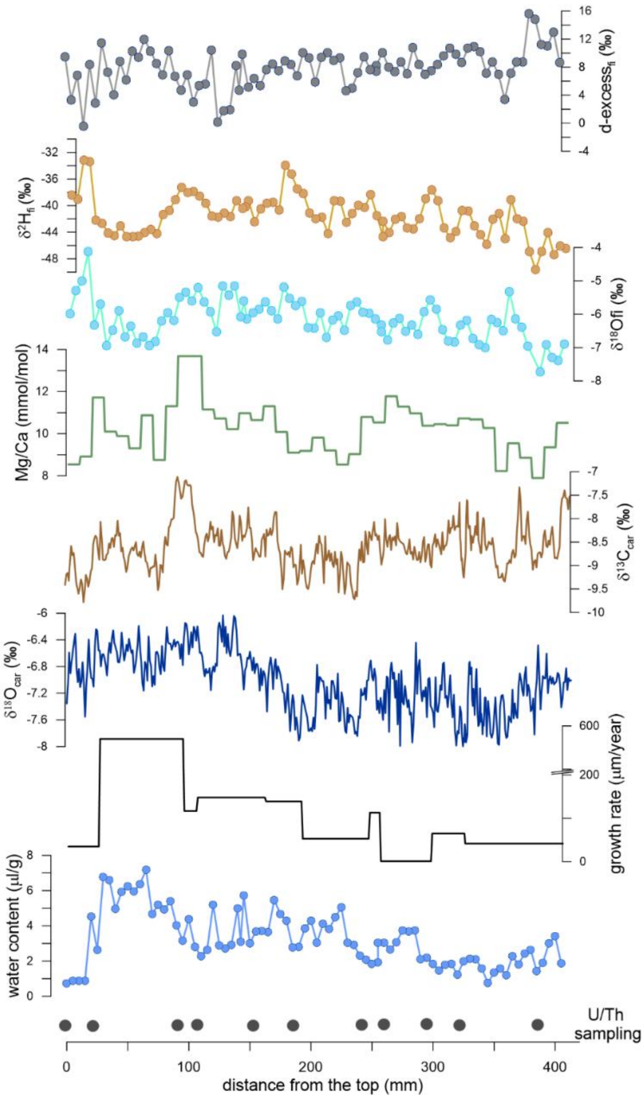

Figure 3. Oxygen isotopes and d-excess in fluid inclusions (fi), oxygen and carbon isotopes in carbonate, Mg/Ca ratio and growth rate of stalagmite SM4 with distance from the top.

https://doi.org/10.5194/egusphere-2026-4435
Preprint. Discussion started: 7 August 2026

4.2. U-Th dating

^{238}U content in the eleven analyzed samples from SM4 range from 93 to 365 ppb. The $^{230}Th/^{232}Th$ activity ratio, critical for the reliability of the final ages, is relatively high (>440·10-6 atomic ratio), indicating low detrital thorium contamination. As a result, the ^{232}Th corrected age differs by less than 1% to the "uncorrected" ages. The age of the analyzed samples ranges from 4,621±12 at 70 mm from the top, to 9,244±50 yr BP at 399 mm (Fig. 2). The average age error is 0.5% of the age, ranging from 12 to 62 years. No age reversal is observed within analytical errors. The growth rate of stalagmite SM4 range from low values of approximately 1 µm yr^{-1} at around 7.2 ka to high calcite precipitation rates of up to 570 µm yr^{-1} at approximately 5.4 ka. Overall, growth rates show an increasing trend from about 6.0 ka to 5.4 ka.

4.3. Oxygen and carbon stable isotopes and Mg/Ca in carbonate

The $\delta^{18}O_{carb}$ values of carbonate in SM4 range from −5.81 to −8.51‰, while $\delta^{13}C$ values range from −7.11 to −9.78‰. The most striking feature of the record is a gradual increase in both isotope ratios between ~240 and ~140 mm from the top of the speleothem (ca. 6.4–5.6 ka), amounting to ~1.5‰ for $\delta^{18}O_{carb}$ and ~1.7‰ for $\delta^{13}C$. The correlation between $\delta^{18}O_{carb}$ and $\delta^{13}C$ over the entire record is weak ($R^2 = 0.12$); however, it increases markedly when only the 240–140 mm interval is considered ($R^2 = 0.49$).

Mg/Ca ratios range from 7.9 to 13.7 mmol/mol and display a pattern similar to $\delta^{13}C$ and broadly similar to that of $\delta^{18}O_{carb}$. A gradual increase in Mg/Ca is also observed between 240 and 140 mm, coinciding with the isotopic shifts in $\delta^{18}O_{carb}$ and $\delta^{13}C$ (Fig. 3). This pattern is consistent with the increase in carbonate precipitation rates observed between ca. 6.0 and 5.4 ka.

4.4. Stable isotopes in fluid inclusions

The oxygen isotope composition of fluid inclusions ($\delta^{18}O_{fi}$) ranges from -4.1 to -8.2‰, while the hydrogen isotope composition (δ^2H) ranges from −49.6 to −33.1‰. The d-excess values of water in the fluid inclusions varies between 0.4 and 15.7‰. The $\delta^{18}O_{fi}$ and δ^2H values define a linear relationship described by $\delta^2H = 4.2 \cdot \delta^{18}O_{fi} - 15.8$ ($R^2 = 0.77$). The isotopic composition of the fluid inclusions closely matches that of rainwater in Almería during the wet season (November to May) (Fig. 4), as well as that of groundwater from the Sierra de Gádor (Vandenschrick et al., 2002; García-López et al., 2022). Most fluid-inclusion values plot along the Global Meteoric Water Line, which, in turn, aligns with rainwater isotope values at the Almería airport (IAEA/WMO, 2026) (Fig. 4).

The $\delta^{18}O_{fi}$ values show a gradual increase from the base to the top of the stalagmite of approximately 1‰, rising from mean values of −7‰ to −6‰ (Fig. 3). Similarly, δ^2H values increase by about 8‰, from around −46‰ to −38‰. In contrast, d-excess values decrease through time, from mean values of ~10‰ at around 9.3 ka to ~6‰ by 4.8 ka (Fig. 3). The $\delta^{18}O$ and

https://doi.org/10.5194/egusphere-2026-4435
Preprint. Discussion started: 7 August 2026

δ^2H values reach their minimum values of the record (−8.2 and −50‰, respectively) at 8.9 kyr BP. The δ^{18}O and δ^2H values are slightly higher at that time than modern groundwater values in Sierra de Gádor (−9.4±0.5‰ and −59±2.5‰, respectively; García-Lopez et al., 2023). This is likely because the recharge altitude of the groundwater is higher than the altitude at which Simarrón II cave is located, above 1,500 m a.s.l (Vallejos et al., 1997). Thus, the $\delta^{18}O_{fi}$ and δ^2H of the SM4 stalagmite cannot be directly compared to those of modern groundwater.

The water content in calcite varied markedly along the speleothem, ranging from 0.7 to 7.2 µL g^{-1}. It shows a gradual increase from the base of the speleothem up to approximately 50 mm below the top, followed by a decrease to minimum values within the uppermost 20 mm. Maximum water content coincides with peak growth rates and highest Mg/Ca at around 5.3 ka (Fig. 3).

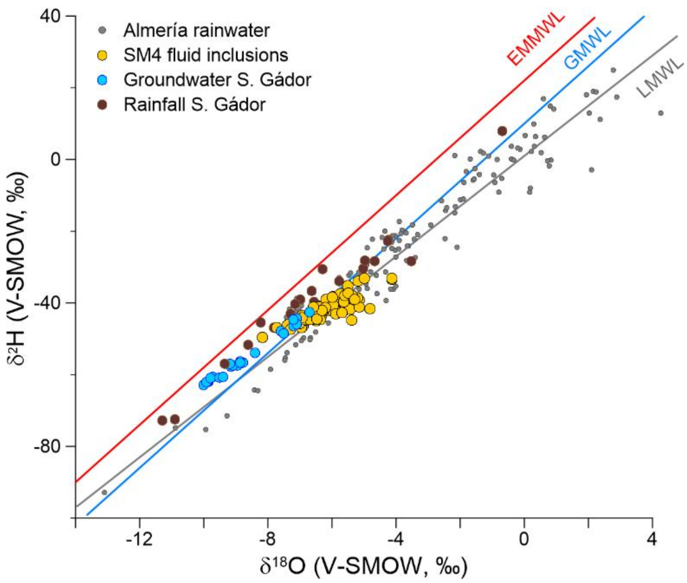

Figure 4. Oxygen and hydrogen stable isotope composition of fluid inclusions in stalagmite SM4. The Global Meteoric Water line (GMWL), the Eastern Mediterranean Meteoric Water Line (EMMWL), rainfall waters at Almería airport from IAEA/WMO (2026) and Sierra de Gádor (Araguas, 1991; García-López et al., 2022) are displayed for comparison. Also, the isotopic composition of groundwater (springs) in Sierra de Gádor is plotted after Vandenschrick et al., (2002) and García-López et al., (2022).

4.5. TEX_{86} paleotemperatures

The TEX_{86} paleotemperatures calculated for the SM4 stalagmite in the period from 9.3±0.2 to 5.0±0.1 ka, ranged from 13.7 to 17.2 ºC with a mean value of 15.7 ºC. The highest temperature value is observed at 5.5 ka, while the lowest temperature occurred at 9.3 ka. These temperatures are higher than those observed in the modern cave atmosphere (e.g. 11.9 °C in September 2005 to 11.2 °C in January 2006; Mayoral et al., 2022).

https://doi.org/10.5194/egusphere-2026-4435
Preprint. Discussion started: 7 August 2026

5. Discussion

5.1. Hydroclimate controls on the SM4 geochemical proxies

Under ideal conditions of carbonate precipitation in caves, the $\delta^{13}C$ of calcite generally reflects changes in soil productivity and/or vegetation type (C3 vs. C4 plants) and vegetation density, whereas $\delta^{18}O_{carb}$ is primarily controlled by variations in the isotopic composition of seepage water (i.e., rainfall) and/or long-term in-cave temperature. However, several processes can modify the original climate signal during its transfer to speleothems, operating within the soil, the epikarst, or the cave atmosphere (e.g., Fairchild et al., 2006).

Ideal conditions for speleothem precipitation include, among others, a water-saturated cave atmosphere (i.e., ~100% relative humidity), which prevents dripwater from becoming supersaturated with respect to calcite due to evaporation, so that speleothem precipitation occurs mainly through slow CO_2 degassing. Such conditions are difficult to achieve in caves located in semiarid regions, such as Simarrón II cave, where in-cave relative humidity generally does not exceed 90% and can drop to <65% during certain periods of the year (e.g. Gázquez et al., 2017; Ruíz-Caballero et al., 2024). Low relative humidity can affect speleothem precipitation by increasing supersaturation through solution evaporation, leading to rapid carbonate crystallization. Also, evaporation modifies the isotopic composition of dripwater, resulting in higher $\delta^{18}O$ water values that impact the $\delta^{18}O_{carb}$ of speleothems (e.g., Markowska et al., 2020). In parallel, prior calcite precipitation (PCP) can occur. This is a process known to alter the isotopic composition of dissolved HCO_3^- in the epikarst through carbonate precipitation within conduits before seepage water reaches the cave. Alternatively, PCP could also happen on the cave ceiling, especially if the drip rate is very slow. PCP affects both the isotopic composition of HCO_3^- and the molar ratios of calcium relative to other elements (e.g., Mg/Ca) (Fairchild and McMillan, 2007). Solution supersaturation driven by rapid CO_2 degassing and in-cave evaporation, as well as enhanced prior calcite precipitation (PCP), are typically associated with dry climatic conditions (Deininger et al., 2021; Patterson et al., 2024). They strongly affect $\delta^{13}C$, generally leading to higher values than those observed under near-equilibrium precipitation conditions, and also result in elevated Mg/Ca ratios in speleothem calcite, in the absence of alternative Mg sources (Fairchild and McMillan, 2007). Consequently, $\delta^{13}C$ and Mg/Ca tend to covary along the speleothem growth axis during dry periods and strong PCP effects.

In the SM4 record, variability in Mg/Ca closely follows that of $\delta^{13}C$ (Fig. 3). Moreover, both parameters show a similar pattern to the speleothem growth rate, suggesting that the kinetics of carbonate precipitation exert primary control on Mg/Ca and $\delta^{13}C$. In this context, higher values of both proxies reflect faster calcite precipitation driven by increasingly dry conditions. Rapid calcite precipitation during dry periods could result from lower infiltration, causing slow dripwater rate and higher oversaturation with respect to $CaCO_3$. An evident period of increasing growth rate is attested between 240 and 140 mm from the speleothem top (Fig. 3); rapid calcite crystallization may result in more porous fabrics with abundant intercrystalline voids,

https://doi.org/10.5194/egusphere-2026-4435
Preprint. Discussion started: 7 August 2026

which are more prone to trapping water as fluid inclusions (López-Elorza et al., 2021). Consistent with this interpretation, the water-content profile of SM4 derived from fluid-inclusion analyses shows a strong correspondence with the speleothem growth rate (Fig. 3), reinforcing the link between rapid calcite precipitation and increased water entrapment.

The $\delta^{18}O_{carb}$ shows a relatively weak correlation with $\delta^{13}C$ when the entire record is considered ($R^2 = 0.12$), suggesting different long-term controls on these two parameters. Indeed, $\delta^{18}O$ and $\delta^{13}C$ are affected differently by kinetic processes, but tend to correlate only when kinetic effects are strong (Fairchild and McMillan, 2007). In this respect, the $\delta^{18}O$-$\delta^{13}C$ correlation in SM4 increases markedly between 240 and 140 mm from the speleothem top ($R^2 = 0.49$), providing evidence for enhanced kinetic fractionation influencing both isotope systems in the context of an overall aridification trend.

Beyond kinetic effects, $\delta^{18}O_{carb}$ may also reflect temperature-dependent oxygen isotope fractionation (e.g., Tremaine et al., 2011) and/or variations in the isotopic composition of dripwater, either directly inherited from precipitation or modified by in-cave evaporation. Although higher cave temperatures generally result in carbonate with lower $\delta^{18}O$ values, TEX_{86}-based temperature reconstructions from stalagmite SM4 indicate that the highest cave temperatures did not coincide with the lowest $\delta^{18}O$ values recorded by the carbonate (Fig. 5). Instead, the two variables appear to be positively correlated, suggesting that temperature effect on oxygen fractionation factor during carbonate precipitation was not the primary control on the $\delta^{18}O$ values of SM4.

Around the Mediterranean, speleothem $\delta^{18}O_{carb}$ primarily records variations in dripwater $\delta^{18}O$, reflecting long-term changes in precipitation isotopic composition (Columbu et al., 2022; Zanchetta et al., 2026), while the effect of cave precipitation temperature is minor (Parker et al., 2021). For SM4, the isotopic composition of dripwater was reconstructed for the interval 9.7–4.4 ka BP using fluid inclusion analyses. We observed that the gradual ~1.5‰ increase observed in $\delta^{18}O_{fi}$ over this period is not mirrored in the $\delta^{18}O_{carb}$ record. Likewise, other prominent features in the $\delta^{18}O_{carb}$ profile, such as the increasing trend from 240 and 140 mm from the speleothem top, are absent from the reconstructed dripwater isotope composition record. These observations suggest that, at least during intervals when $\delta^{18}O_{carb}$ and $\delta^{13}C$ covary, both proxies were dominantly influenced by kinetic effects linked to carbonate growth rates, rather than by changes in water isotope composition. In turn, growth-rate variations were likely controlled by changes in drip rate and/or cave ventilation.

https://doi.org/10.5194/egusphere-2026-4435
Preprint. Discussion started: 7 August 2026

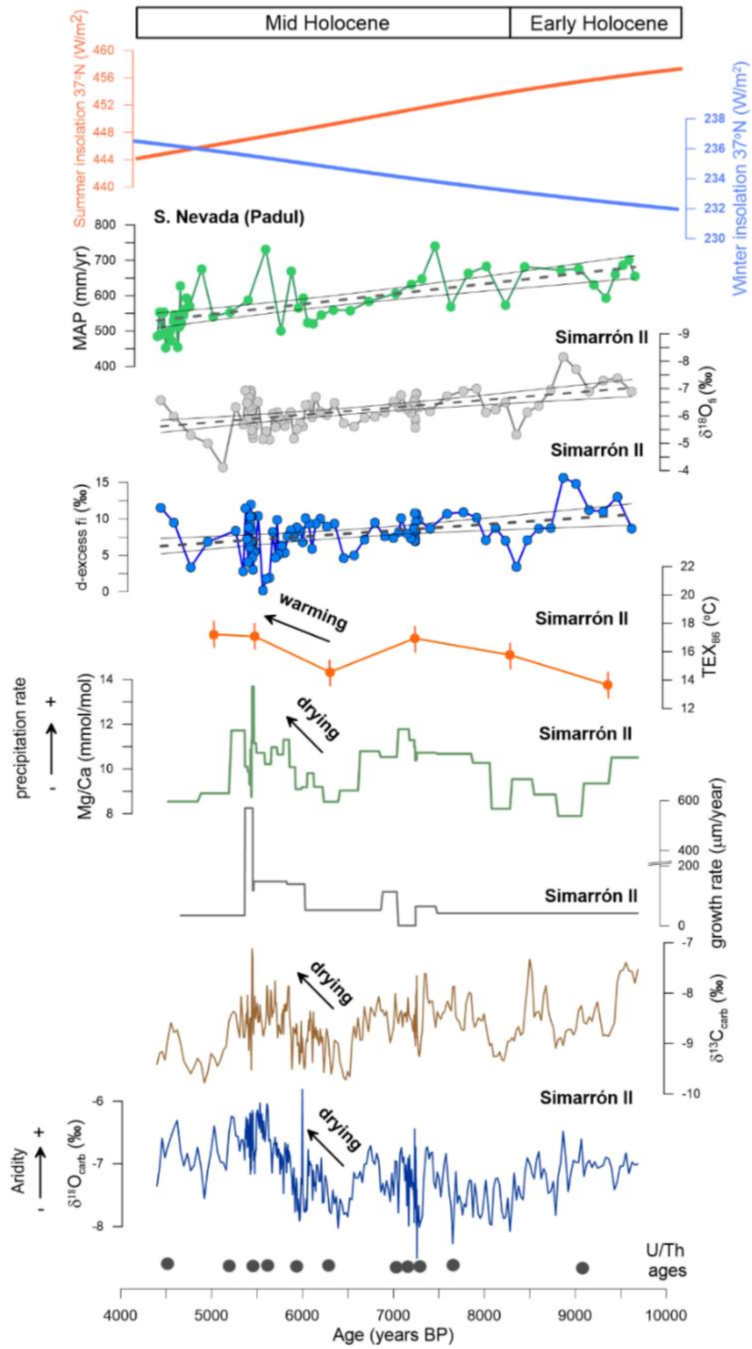

Figure 5. Comparison of the oxygen and carbonate isotopes in carbonate, Mg/Ca ratio (z-score standardization) with TEX_{86} temperatures and $\delta^{18}O$ and d-excess in fluid inclusions in stalagmite SM4 (without potential evaporation artifact correction) with insolation at 37°N and a record of Mean Annual Precipitation in Sierra Nevada mountain range (Camuera et al., 2022).

https://doi.org/10.5194/egusphere-2026-4435
Preprint. Discussion started: 7 August 2026

In summary, periods of accelerated carbonate precipitation in Simarrón II cave are characterized by higher Mg/Ca ratios and higher $\delta^{13}C$ values in the SM4 stalagmite. Enhanced growth rates likely reflect higher solution supersaturation, because of enhanced CO_2 degassing and/or increased evaporation under relatively dry climatic conditions. Therefore, the Mg/Ca ratios $\delta^{13}C$ values can be mostly used as paleo-aridity proxies. The $\delta^{18}O_{carb}$ signal is likely modulated by the same mechanisms associated with changes in aridity, but it is also influenced by variability in the $\delta^{18}O$ of dripwater and, to a lesser extent, by changes in cave temperature. Finally, the increasing trend observed in $\delta^{18}O$ and $\delta^{2}H$ throughout the speleothem can be related to the long-term evolution of the isotopic composition of rainfall in the southern Iberian Peninsula between 9.7 and 4.4 ka, overprinted by evaporation processes occurring either outside or inside the cave. Notably, these increases in $\delta^{18}O$ and $\delta^{2}H$ in dripwater are accompanied by a gradual decrease in d-excess. This pattern may reflect a long-term decline in the d-excess of precipitation linked to changes in moisture source and in the dominant precipitation regimes, shifting between convective Mediterranean-type rainfall and advective Atlantic frontal systems (Stachnik et al., 2016). However, enhanced evaporation from 9.7 to 4.4 ka, either in the soil zone prior to infiltration into the epikarst or within the cave itself, would produce a similar isotopic signature, resulting in higher $\delta^{18}O$ and $\delta^{2}H$ values and lower d-excess in dripwater (Warken et al., 2022). Consequently, the isotopic composition of fluid inclusions in the SM4 speleothem is interpreted with caution, as both long-term changes in rainfall isotopic composition and variations in in-cave evaporation driven by paleo-aridity could have controlled the isotopic composition of dripwater in Simarrón II cave during this interval.

5.2. Paleotemperature estimates from SM4 stalagmite

To reconstruct paleotemperatures from the SM4 stalagmite, two independent approaches were adopted: (1) paired $\delta^{18}O_{carb}$–$\delta^{18}O_{fi}$ measurements and (2) TEX_{86} analyses. For the first method, we applied the paleothermometer equation proposed by Tremaine et al. (2011), which was specifically developed for cave environments. Studies of the stable isotopic composition of speleothem fluid inclusions using the "crushing" method, as employed in the present study, have shown that evaporation during crushing may affect isotopic results, particularly when the amount of released water is small (Fernández et al., 2023). However, this analytical artifact can be corrected using a mathematical approach that assumes a constant evaporation $\delta^{18}O$- $\delta^{2}H$ slope and the intercept with the Global Meteoric Water Line (GMWL) (see Fernández et al., 2023 for details). This correction assumes that the original isotopic composition of fluid inclusion waters plots on the GMWL and that deviations from this line result from evaporation during sample processing. Alternatively, it may be assumed that fluid inclusion waters before water evaporation in the crusher plotted on the Local Meteoric Water Line (LMWL). In the case of Almería ($\delta^{2}H = 6.9 \times \delta^{18}O + 1.5$), the LMWL differs significantly from the GMWL; thus, this difference has also been considered.

When the Tremaine et al. (2011) paleotemperature equation is applied without correcting $\delta^{18}O_{fi}$ for potential analytical artifacts, temperatures derived from paired $\delta^{18}O_{carb}$–$\delta^{18}O_{fi}$ measurements range from 15 to 35°C, with a mean value of 25±3°C.

https://doi.org/10.5194/egusphere-2026-4435
Preprint. Discussion started: 7 August 2026

These values are considerably higher than modern cave temperatures, which ranged from 11.2°C in January 2006 to 11.9°C in September 2005 (Mayoral et al., 2022) and appear unrealistically high for a cave located at ~1,500 m a.s.l. at 36.5° latitude, even during relatively warm climatic periods.

Applying the correction proposed by Fernández et al. (2023) reduces the temperature range to 20–33°C, although the mean temperature remains largely unchanged (26±2°C). Similarly, when the LMWL is used instead of the GMWL for the correction, calculated temperatures also range from 20 to 33°C, with a mean value of 24±3°C (Fig. 6). In all cases, the correction fails to produce temperatures approaching expected cave conditions. This suggests that the anomalously high temperatures obtained from paired $\delta^{18}O_{carb}$- $\delta^{18}O_{fi}$ measurements are not primarily caused by analytical artifacts during fluid inclusion analysis, but rather by non-equilibrium processes during calcite precipitation, such as rapid CO_2 degassing and water evaporation within the cave. Higher $\delta^{18}O$ values of water trapped in fluid inclusions are also expected if seepage water underwent evaporation, either in the soil, epikarst, or the cave atmosphere (Warken et al., 2022). Indeed, for a given $\delta^{18}O_{carb}$ value, a 1‰ increase in $\delta^{18}O_{fi}$ results in a calculated paleotemperature that is approximately 6°C higher. Because the present-day relative humidity in Simarrón II cave rarely reaches 100% and can occasionally decrease to 65–70%, some degree of evaporation likely occurred during the formation of the SM4 stalagmite. This effect may have been particularly pronounced during drier intervals, when lower cave humidity would have enhanced evaporative isotopic enrichment of seepage waters prior to calcite precipitation. Consequently, paleotemperatures derived from this approach are considered unreliable and are not used for paleoclimatic interpretation in this study.

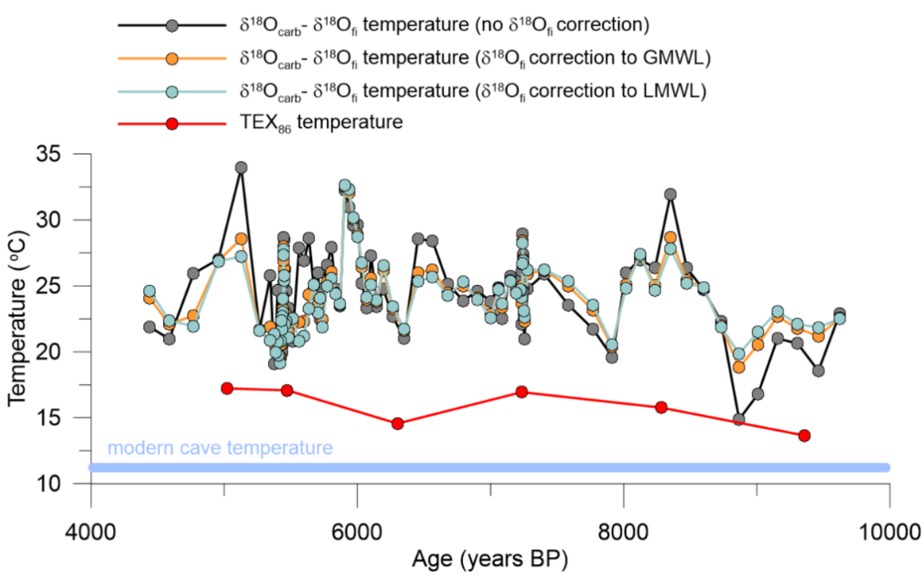

https://doi.org/10.5194/egusphere-2026-4435
Preprint. Discussion started: 7 August 2026

Figure 6. Paleotemperature estimates derived from the equation of Tremaine et al. (2011) using $\delta^{18}O$ values from carbonate and fluid inclusions in stalagmite SM4. Different calculation approaches were applied, including: (i) no correction of $\delta^{18}O_{fi}$ values by potential evaporation artifact in the crusher; (ii) correction by potential evaporation artifact in the crusher to the Global Meteoric Water Line (GMWL) following the approach of Fernández et al. (2023); and (iii) the same type of correction but using the Local Meteoric Water Line (LMWL) for Almería. Temperatures reconstructed from the TEX_{86} proxy are also shown and compared with the present-day cave temperature.

The TEX_{86} method yielded temperatures ranging from 13.7 to 17.2 °C, with a mean value of 15.7 °C. These estimates are substantially closer to modern cave temperatures (Fig. 6). The results indicate that temperatures reached up to ~17 °C during the Mid-Holocene (at 7.2, 5.5, and 5.0 ka), whereas cooler conditions prevailed during the Early Holocene, with temperatures as low as 13.7 °C at 9.3 ka. Although TEX_{86} paleotemperature reconstructions rely on a transfer function that may not be universally applicable to all cave systems, relative temperature variations between samples are likely robust. Despite the limited number of TEX_{86} measurements, the data indicate that temperatures at 6.3 ka were approximately 2.5°C lower than those recorded at 7.2, 5.5, and 5.0 ka. Importantly, this cooler interval coincides with wetter conditions inferred from the $\delta^{18}O_{carb}$, $\delta^{13}C$, and Mg/Ca proxies (Fig. 5). Subsequently, between 6.4 and 5.6 ka, these proxies indicate a shift towards more arid conditions, while TEX_{86}-derived temperatures increased by approximately 2.5°C. Taken together, these results suggest that the termination of the last nAHP in the setting of Simarrón II cave was characterized by relatively rapid climatic oscillations, with wetter and cooler conditions peaking around 6.4 ka, followed by a transition towards warmer and drier conditions marking the end of the humid phase at around 5.5 ka. Indirect evidence of this aridity trend might be the potential hiatus detected at 30 mm from the stalagmite top and just above the age of 5,364±38 yr BP (Fig. Sup. 1). However, as speleothem hiatuses can be driven by multiple processes not necessarily linked to aridity (Columbu et al., 2025; Pérez-Mejías et al., 2025), this feature is considered only as ancillary evidence and is not further discussed.

5.3. Comparing the SM4 record with other regional paleoclimate records

5.3.1. Iberian and northern Maghreb speleothem records

Over the last decades, numerous speleothem records spanning the Early and Middle Holocene have become available from northwestern Africa and the Iberian Peninsula. To place the Simarrón II cave record in a broader regional context, the SM4 $\delta^{18}O_{carb}$ profile is compared with some of these western Mediterranean speleothem records, after standardizing the datasets using z-scores (Fig. 7). In most of these previous studies, speleothem $\delta^{18}O_{carb}$ values have been interpreted primarily as reflecting changes in hydroclimatic conditions, particularly variations in aridity, rather than temperature, with higher z-score values indicating drier conditions and lower values indicating wetter conditions. A similar interpretation is adopted for the SM4 record, as discussed in section 5.1.

https://doi.org/10.5194/egusphere-2026-4435
Preprint. Discussion started: 7 August 2026

Overall, most speleothem records indicate the onset of the driest Holocene conditions occurred between approximately 6 and 5 ka, coinciding with the termination of the last nAHP (Fig. 7). The Early Holocene prior to 8.5 ka was generally characterized by relatively drier conditions, while the interval between 8.5 and 6 ka appears to represent the wettest phase in most records. Nevertheless, most records exhibit a temporary return to more arid conditions during the Middle Holocene, between approximately 6.5 and 5.5 ka, as indicated by positive $\delta^{18}O_{carb}$ z-score values (Fig. 7). This pattern suggests that the wettest phases of the Holocene in the western Mediterranean region occurred around 8.0 ka and 6.5 ka, separated by a relatively drier phase. The climatic mechanism responsible for these wetter stages of the Holocene responded to persistent negative North Atlantic Oscillation (NAO)-like configuration resulting from a weakening of the Subpolar Gyre and an enhanced Subtropical Gyre, with possibly the combination with other atmospheric modes (Luppichini et al., 2026). This atmospheric pattern promoted a southward displacement of the North Atlantic westerly storm tracks, leading to increased winter precipitation across the western Mediterranean region (Ait Brahim et al., 2019).

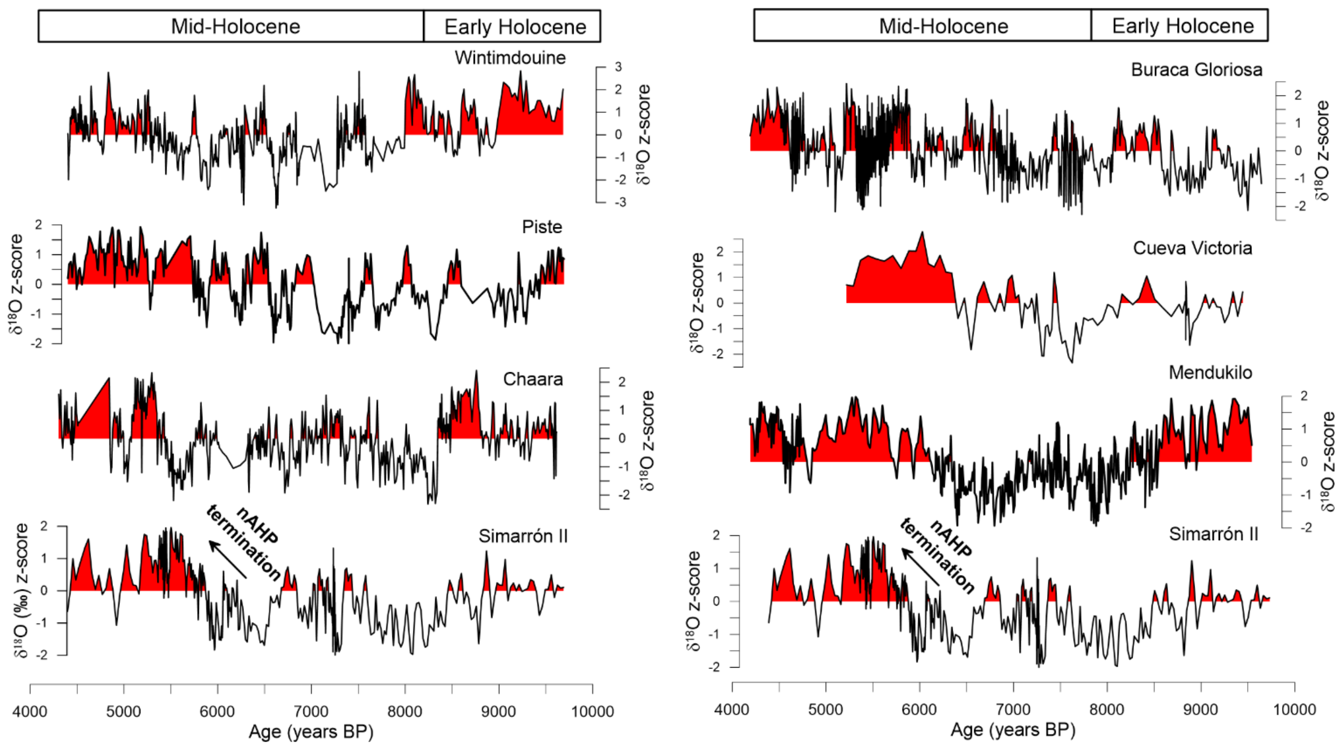

Figure 7. Comparison of $\delta^{18}O$ isotopes in carbonate (z-score) of stalagmite SM4 from Simarrón II cave with other stalagmites of Morocco (left, including Wintimdouine, Piste and Chaara caves, by Sha et al., 2019; Wassenburg et al., 2016 an Ait Brahim et al., 2019, respectively) and the Iberian Peninsula (right; including Buraca Gloriosa, Cueva Victoria and Mendukilo caves by Thatcher et al., 2020, Budsky et al., 2019 and Bernal-Wormull et al., 2023, respectively).

In particular, the Cueva Victoria speleothem record (40 m a.s.l.; Budsky et al., 2019), located less than 200 km from Simarrón II Cave, suggests atmosphere reorganization and climate change associated with the termination of the last nAHP occurred between 6.5 and 6.0 ka, approximately 500 years earlier than inferred from the SM4 stalagmite. This discrepancy may be related to the contrasting elevations of the two sites. Whereas Simarrón II cave is located at approximately 1500 m a.s.l., Cueva Victoria is situated near sea level. This observation suggests that the effects of regional aridification may have been delayed at higher elevations in southeastern Iberia, allowing relatively humid environments to persist as climatic refugia during the final stages of the last nAHP. Note that also uncertainties in the geochronological model of the Cueva Victoria speleothems for some period may be responsible for some discrepancies. This drying trend is also recorded in the $\delta^{18}O_{carb}$ speleothem record from Molinos Cave in northeastern Spain, where a progressive increase in $\delta^{18}O_{carb}$ values between ~6.5 and 5 ka has been interpreted as reflecting increasingly arid conditions (Moreno et al., 2017). Similarly, speleothem density records from El Refugio Cave in southern Spain indicate increasingly variable drip rates beginning at ~5.3 ka, likely reflecting enhanced seasonality and generally drier conditions. This shift was preceded by the wetter conditions that characterized the Holocene Climatic Optimum (Walczak et al., 2015).

The SM4 record does not provide evidence for increased aridity during the so-called 8.2 ka cold event. On the contrary, the some of the lowest $\delta^{18}O_{carb}$ values of the entire record are observed during this interval, suggesting particularly humid conditions. This observation is consistent with the heterogeneous spatial expression of the 8.2 ka event across the Iberian Peninsula. While clear hydroclimatic responses have been documented in southwestern Iberia (Schröder et al., 2018) and northern Iberia (Rossi et al., 2018; Baldini et al., 2019), evidence for this event remains elusive in most paleoclimate archives from southeastern Iberia (e.g. Ramos-Román et al., 2018; among others).

The ~2.5 °C temperature increase inferred from the TEX_{86} proxy during the final stages of the nAHP coincides with the onset of drier conditions recorded by all speleothem records considered in this comparison. The termination of the last nAHP seems to have been primarily driven by a decline in Northern Hemisphere summer insolation associated with orbital precession, which weakened the African monsoon and reduced moisture transport into the Sahara (Fig. 5) (deMenocal et al., 2000). Vegetation-atmosphere and dust feedback likely amplified this transition, resulting in a rapid shift toward arid conditions across much of North Africa (Claussen et al., 1999). Comparison of speleothem records from the Iberian Peninsula and the northern Maghreb indicates that the precise timing of the final nAHP termination in the western Mediterranean varied by up to approximately ±500 years among sites. Nevertheless, all records consistently document a progressive shift toward drier conditions, highlighting the regional expression of a large-scale climatic transition, not only in norther Africa, but also in southern Europe.

https://doi.org/10.5194/egusphere-2026-4435
Preprint. Discussion started: 7 August 2026

5.3.2. Comparison with other southern Iberian non-speleothem records

Although paleoclimate records derived from speleothems in southern Iberia are still relatively scarce, a considerable number of Holocene paleoclimate reconstructions are available from other archives. This includes alpine lakes and peat bogs from several mountain ranges (Jimenez-Moreno et al., 2026 and references therein), and marine sediments from the Alboran Sea (Cacho et al., 1999; Rodrigo-Gámiz et al., 2014).

Reconstructions of mean annual precipitation (MAP) from pollen records in the Padul peat bog (740 m a.s.l.) indicate a gradual decline in precipitation across southeastern Iberia during the Early and Middle Holocene (Camuera et al., 2022), amounting to approximately 20%, from about 700 to 550 mm yr^{-1} between 9.5 and 5 ka. This long-term trend toward increasing aridity is consistent with that observed in the fluid inclusion water isotopes of stalagmite SM4, which display progressively increasing $\delta^{18}O_{fi}$ and $\delta^{2}H$ values over the same period, accompanied by an increase in d-excess. The widespread shift toward drier climatic conditions may have enhanced evaporation of infiltrating waters both before entering the cave system, within the soil and epikarst, and potentially within the cave itself. In addition, under a drier and likely more Mediterranean-type climate, characterized by a more irregular seasonal distribution of rainfall, fewer frontal precipitation events, and a greater contribution from convective storms, higher $\delta^{18}O$ and $\delta^{2}H$ values in precipitation are expected in this region. Recent studies of modern precipitation in Iberia support this interpretation, showing isotopically depleted rainfall associated with Atlantic moisture sources and isotopically enriched rainfall associated with convective Mediterranean-derived rainfall (Gimenez et al., 2021; Stachnick et al., 2026). Also, changes in moisture source have previously been proposed as an important control on the isotopic composition of precipitation during the Holocene in this region (Toney et al., 2020; García-Alix et al., 2021).

The aridification of the Sahara during the termination of the last nAHP was recorded also in the sediments of Laguna de Río Seco (3020 m a.s.l.) in the Sierra Nevada range, barely 40 km apart from Sierra de Gádor, as an increase in the Zr/Th ratio, reflecting enhanced Saharan dust input that progressively intensified between 7 and 5 ka (Fig. 8) (Jiménez-Espejo et al., 2014). However, this lake record also shows a minimum in organic matter $\delta^{13}C$ values at 6.2 ka, suggesting enhanced productivity within the catchment during this interval. This productivity maximum coincides with minima in both $\delta^{18}O_{carb}$ and $\delta^{13}C$ values recorded in stalagmite SM4 from Simarrón II cave, reinforcing the interpretation of relatively humid conditions prior to the end of the nAHP. A sharp increase in the C/N ratio of this lake sediments at 5.5 ka has been linked to a substantial shift in the dominant source of organic matter in the lake, from predominantly algal to a greater contribution from vascular plants (Fig. 8). This likely reflects a major environmental change that reduced algal productivity, most probably a decrease in lake level associated with increasing aridity (Jiménez-Espejo et al., 2014). Similarly, palynological records from several lakes in this sector of the Iberian Peninsula document a transition from mesophytic and hygrophytic taxa to xerophytic vegetation between 5.9 and 5.4 ka (Carrión, 2002; Carrión et al., 2003).

https://doi.org/10.5194/egusphere-2026-4435
Preprint. Discussion started: 7 August 2026

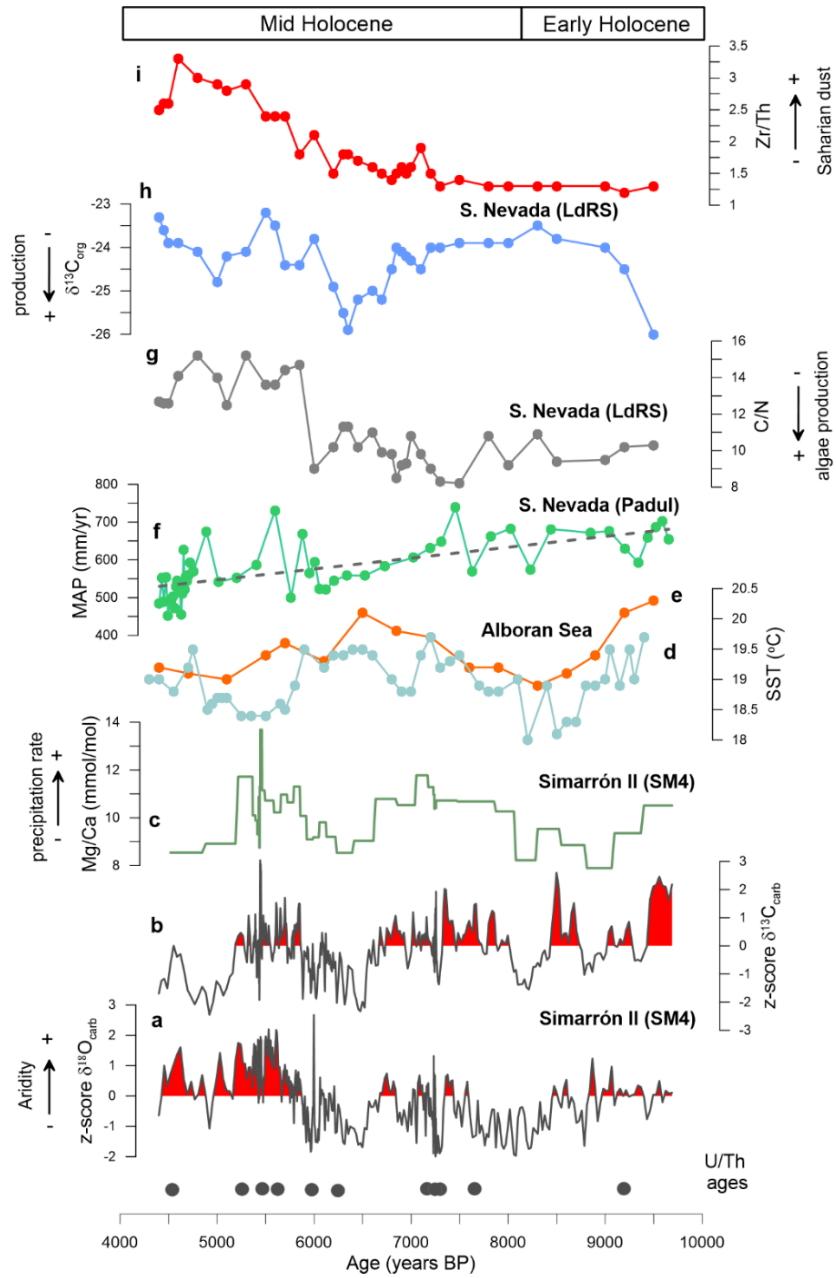

Figure 8. Comparison of the $\delta^{18}O/\delta^{13}C$ (a and b) and Mg/Ca (c) in calcite of stalagmite SM4 with other non-speleothem paleoclimate records of the SE Iberian Peninsula, including Sea Surface Temperatures (SST) reconstructed from UK'37 index (d; Cacho et al., 1999; e. Rodrigo-Gámiz et al., 2014), mean annual precipitation (MAP) reconstructed from pollen data reanalysis (Camuera et al., 2022) and organic and inorganic proxies from Laguna de Ríos Seco lake in Sierra Nevada (Jiménez-Espejo et al., 2014).

https://doi.org/10.5194/egusphere-2026-4435
Preprint. Discussion started: 7 August 2026

In general, the TEX_{86} record from the SM4 stalagmite does not closely match marine sea-surface temperature (SST) reconstructions from the Alboran Sea. The Simarrón II stalagmite records relatively high temperatures (~17 °C) around 7.2 ka and again after ~5.5 ka. Between these intervals, however, temperatures decreased to ~14.5 °C immediately before the termination of the last nAHP, implying a subsequent warming of approximately 2.5 °C that coincided with the transition to drier conditions (Figs. 5 and 6). In contrast, SST reconstructions from the Alboran Sea indicate persistently warm conditions between ~8 and 6 ka, followed by cooling during the end of the nAHP (Cacho et al., 1999; Rodrigo-Gámiz et al., 2014). This discrepancy suggests that the TEX_{86} signal in SM4 is influenced by local environmental factors, including hydroclimate-driven changes or effects associated to vegetation cover that may result in in local cooling/warming. For instance, changes in the surface albedo above the cave may have resulted in long-term changes in the mean annual temperature of the ground and epikarst, which could have been transmitted to the cave interior.

Most paleotemperature records spanning the Middle-to-Late Holocene transition indicate a gradual cooling trend across the western Mediterranean beginning at ~6-7 ka, primarily driven by the progressive decline in Northern Hemisphere summer insolation at 37°N (e.g., Jiménez-Moreno et al., 2023, 2025). Nevertheless, several records reveal superimposed shorter-term warming episodes. For example, chironomid-based reconstructions from the Sierra Nevada suggest an increase in summer air temperature of approximately 1 °C between ~7 and 5 ka, despite the overall long-term cooling trend (Jiménez-Moreno et al., 2025). A comparable mid-Holocene temperature recovery has also been inferred from lake sediments in the Alps (Heiri et al., 2015). Therefore, the warming recorded by TEX_{86} in SM4 during the final stages of the nAHP is qualitatively consistent with evidence from other terrestrial paleotemperature archives across southern Europe.

6. Conclusions

The multi-proxy record obtained from stalagmite SM4 from Simarrón II cave provides one of the most comprehensive terrestrial reconstructions of hydroclimatic and environmental changes across the termination of the last North African Humid Period in southeastern Iberia. By combining carbonate and fluid inclusion stable isotopes with TEX_{86}-derived temperature estimates, this study offers new insights into the evolution of regional climate between ~9.5 and 5 ka and into the climatic links between southern Iberia, North Africa and the western Mediterranean.

The different geochemical proxies consistently document a progressive transition from relatively humid conditions during the Early and Middle Holocene towards increasingly arid conditions after ~6 ka. Carbonate $\delta^{18}O$ and $\delta^{13}C$ values, together with the isotopic composition of fluid inclusion waters, reveal a long-term reduction in effective moisture that culminated between ~5.8 and 5.3 ka, marking the establishment of the driest conditions recorded in the sequence. The parallel increase in fluid inclusion $\delta^{18}O$, $\delta^{2}H$ and decrease in d-excess suggests that this hydroclimatic transition resulted from a combination of enhanced evaporation, and potentially changes in rainfall seasonality, and a progressive increase in the contribution of

https://doi.org/10.5194/egusphere-2026-4435
Preprint. Discussion started: 7 August 2026

Mediterranean-derived precipitation relative to Atlantic moisture sources. Together, these observations indicate that the termination of the nAHP in southeastern Iberia involved not only a reduction in precipitation amount, but also changes in atmospheric circulation and the hydrological cycle.

Comparison with other speleothem records from the Iberian Peninsula and northern Africa demonstrates that the hydroclimatic transition associated with the end of the nAHP was a regional phenomenon expressed throughout the western Mediterranean, although its precise timing differed among sites by up to several centuries. In particular, the SM4 record suggests that humid conditions persisted longer at high elevations than at lower-altitude sites in southeastern Iberia, implying that mountainous regions acted as climatic refugia during the final stages of Holocene aridification. This highlights the importance of topography in modulating the regional expression of large-scale climatic changes driven by orbital forcing and monsoon dynamics.

Beyond its paleoclimatic implications, the SM4 record provides an important environmental framework for interpreting the Mesolithic–Neolithic transition in southern Iberia. Archaeological evidence indicates that the arrival of the first farming communities during the mid-6th millennium cal BC did not immediately replace Mesolithic lifeways. Instead, hunter-gatherer and early farming economies coexisted for several centuries while domestic plants and animals were progressively incorporated into subsistence strategies (Martínez-Sánchez et al., 2024). This socioeconomic transition occurred during a period of progressive aridification culminating between ~5.8 and 5.3 ka, when reduced effective moisture likely affected freshwater availability, ecosystem productivity and the distribution of natural resources. Although climate change may have not the primary driver of Neolithisation, the establishment of persistently drier conditions probably acted as an important environmental constraint influencing settlement patterns and resource exploitation. The close temporal correspondence between increasing aridity and the gradual shift from seasonal shellfish-gathering and fishing to pastoral land use suggests that Holocene climate deterioration contributed to reshaping the environmental setting in which farming economies became consolidated across southern Iberia.

Data availability

Data of stalagmite SM4 are available at the EU Zenodo repository at doi.**10.5281/zenodo.21498781.**

Author contributions

The authors contributed to the paper as follows: field sampling by FG & JMC; conceptualization by FG; writing the original draft by FG; formal analysis by FG, EI, HV, AMG, CPM, AC, AG & AD; resources by FG, HV, AMG, EI, BD & AC; review and editing by FG, JMC, EI, HV, AMG, CPM, HC, AG & AD; funding acquisition by FGS; and project administration by FG.

Competing interests

The contact author has declared that none of the authors has any competing interests.

Disclaimer

Copernicus Publications remains neutral with regard to jurisdictional claims made in the text, published maps, institutional affiliations, or any other geographical representation in this paper. While Copernicus Publications makes every effort to include appropriate place names, the final responsibility lies with the authors. Views expressed in the text are those of the authors and do not necessarily reflect the views of the publisher.

Acknowledgements

The authors thank the Speleoclub Almería (ECA) for its support during field work. Lucía Martegani and Elvira Ruíz participated in the subsampling of the SM4 speleothem. The authors used an AI-based language model exclusively to improve the English language and readability of the manuscript. No scientific content, analyses, interpretations, figures or conclusions were generated by the AI tool.

Financial support

This research was funded by the Project P_FORT_GRUPOS_2023/17 of the University of Almería and Junta de Andalucía Regional Government through European Union FEDER funds and the funds of the Water Resources and Environmental Geology Group (RNM-189) of University of Almería. Dr. Fernando Gázquez thanks the Ramón y Cajal contract (RYC2020-029811-I), the PPIT-UAL grant from the Junta de Andalucía-FEDER 2022-2026 (RyC-PPI2021-01) and CNS2025-165139 (CLIMGYP) projects of the Ministerio de Ciencia e Innovación of Spain and the Agencia Estatal de Investigación. The “Redes de Investigación" project PALEONET (RED2024-153734-T) of the Agencia Estatal de Investigación facilitated collaboration between the University of Almería and the University of Burgos.

References

Affolter, S., Kipfer, T., Hofmeister, E., Leuenberger, M., and Fleitmann, D.: Paleoclimatic significance of water isotopes in speleothem fluid inclusions, *Earth-Sci. Rev.,* 261, 105026, https://doi.org/10.1016/j.earscirev.2024.105026, 2025.

Ait Brahim, Y., Wassenburg, J. A., Sha, L., Cruz, F. W., Deininger, M., Sifeddine, A., Bouchaou, L., Spötl, C., Edwards, R. L., and Cheng, H.: North Atlantic ice-rafting, ocean and atmospheric circulation during the Holocene: Insights from Western Mediterranean speleothems, *Geophys. Res. Lett.*, 46, 7614–7623, https://doi.org/10.1029/2019GL082405, 2019.

Araguás-Araguás, L.: Adquisición de los contenidos isotópicos (^{18}O y D) de las aguas subterráneas: variaciones en la atmósfera y en la zona no saturada del suelo, PhD thesis, Universidad Complutense de Madrid, Madrid, Spain, 286 pp., 1991.

Baker, A., Blyth, A. J., Jex, C. N., McDonald, J. A., Woltering, M., and Khan, S. J.: Glycerol dialkyl glycerol tetraethers (GDGT) distributions from soil to cave: Refining the speleothem paleothermometer, *Org. Geochem.*, 136, 103890, https://doi.org/10.1016/j.orggeochem.2019.06.011, 2019.

Baldini, L. M., Baldini, J. U. L., McDermott, F., Arias, P., Cueto, M., Fairchild, I. J., Hoffmann, D. L., Mattey, D. P., Müller, W., Nita, D. C., Ontañón, R., García-Moncó, C., and Richards, D. A.: North Iberian temperature and rainfall seasonality over the Younger Dryas and Holocene, *Quat. Sci. Rev.*, 226, 105998, https://doi.org/10.1016/j.quascirev.2019.105998, 2019.

Bernal-Wormull, J. L., Moreno, A., Bartolomé, M., Arriolabengoa, M., Pérez-Mejías, C., Iriarte, E., Osácar, C., Spötl, C., Stoll, H., Cacho, I., Edwards, R. L., and Cheng, H.: New insights into the climate of northern Iberia during the Younger Dryas and Holocene: The Mendukilo multi-speleothem record, *Quat. Sci. Rev.*, 305, 108006, https://doi.org/10.1016/j.quascirev.2023.108006, 2023.

Bernal-Wormull, J. L., Moreno, A., Dublyansky, Y., Spötl, C., Giménez, R., Pérez-Mejías, C., Bartolomé, M., Arriolabengoa, M., Iriarte, E., Cacho, I., Edwards, R. L., and Cheng, H.: Temperature variability in southern Europe over the past 16500 years constrained by speleothem fluid inclusion water isotopes, *Clim. Past*, 21, 1235–1261, https://doi.org/10.5194/cp-21-1235-2025, 2025.

Blyth, A. J. and Schouten, S.: Calibrating the glycerol dialkyl glycerol tetraether temperature signal in speleothems, *Geochim. Cosmochim. Acta*, 109, 312–328, https://doi.org/10.1016/j.gca.2013.02.009, 2013.

Breitenbach, S. F. M., Rehfeld, K., Goswami, B., Baldini, J. U. L., Ridley, H. E., Kennett, D. J., Prufer, K. M., Aquino, V. V., Asmerom, Y., Polyak, V., Cheng, H., Kurths, J., and Marwan, N.: Constructing proxy records from age models (COPRA), *Clim. Past*, 8, 1765–1779, https://doi.org/10.5194/cp-8-1765-2012, 2012.

Budsky, A., Scholz, D., Wassenburg, J. A., Mertz-Kraus, R., Spötl, C., Riechelmann, D. F., Gibert, L., Jochum, K. P., and Andreae, M. O.: Speleothem $\delta^{13}C$ record suggests enhanced spring/summer drought in south-eastern Spain between 9.7 and 7.8 ka – a circum-Western Mediterranean anomaly?, *Holocene*, 29, 1113–1133, https://doi.org/10.1177/0959683619838021, 2019.

Cacho, I., Grimalt, J. O., Pelejero, C., Canals, M., Sierro, F. J., Flores, J. A., and Shackleton, N.: Dansgaard–Oeschger and Heinrich event imprints in Alboran Sea paleotemperatures, *Paleoceanography*, 14, 698–705, https://doi.org/10.1029/1999PA900044, 1999.

Camuera, J., Ramos-Román, M. J., Jiménez-Moreno, G., García-Alix, A., Ilvonen, L., Ruha, L., Gil-Romera, G., González-Sampériz, P., and Seppä, H.: Past 200 kyr hydroclimate variability in the western Mediterranean and its connection to the African Humid Periods, *Sci. Rep.*, 12, 9050, https://doi.org/10.1038/s41598-022-12047-1, 2022.

Carrión, J. S.: Patterns and processes of Late Quaternary environmental change in a montane region of southwestern Europe, *Quat. Sci. Rev.*, 21, 2047–2066, https://doi.org/10.1016/S0277-3791(02)00010-0, 2002.

Carrión, J. S., Fernández, S., Jiménez-Moreno, G., Fauquette, S., Gil-Romera, G., González-Sampériz, P., and Finlayson, C.: Holocene vegetation dynamics, fire and grazing in the Sierra de Gádor, southern Spain, *Holocene*, 20, 1027–1040, https://doi.org/10.1177/0959683610369508, 2010.

Cheddadi, R., Carré, M., Nourelbait, M., François, L., Rhoujjati, A., Manay, R., Ochoa, D., and Schefuß, E.: Early Holocene greening of the Sahara requires Mediterranean winter rainfall, *Proc. Natl. Acad. Sci. U.S.A.*, 118, e2024898118, https://doi.org/10.1073/pnas.2024898118, 2021.

Cheng, H., Edwards, R. L., Hoff, J., Gallup, C. D., Richards, D. A., and Asmerom, Y.: The half-lives of uranium-234 and thorium-230, *Chem. Geol.*, 169, 17–33, https://doi.org/10.1016/S0009-2541(99)00157-6, 2000.

Cheng, H., Edwards, R. L., Shen, C.-C., Polyak, V. J., Asmerom, Y., Woodhead, J., Hellstrom, J., Wang, Y., Kong, X., Spötl, C., Wang, X., and Alexander, E. C.: Improvements in ^{230}Th dating, ^{230}Th and ^{234}U half-life values, and U–Th isotopic measurements by multicollector inductively coupled plasma mass spectrometry, *Earth Planet. Sci. Lett.*, 371–372, 82–91, https://doi.org/10.1016/j.epsl.2013.04.006, 2013.

Claussen, M., Kubatzki, C., Brovkin, V., Ganopolski, A., Hoelzmann, P., and Pachur, H.-J.: Simulation of an abrupt change in Saharan vegetation in the mid-Holocene, *Geophys. Res. Lett.*, 26, 2037–2040, https://doi.org/10.1029/1999GL900494, 1999.

Columbu, A., Spötl, C., Fohlmeister, J., Hu, H. M., Chiarini, V., Hellstrom, J., Cheng, H., Shen, C.-C., and De Waele, J.: Central Mediterranean rainfall varied with high northern latitude temperatures during the last deglaciation, *Commun. Earth Environ.*, 3, 181, https://doi.org/10.1038/s43247-022-00521-5, 2022.

Columbu, A., Pérez-Mejías, C., Regattieri, E., Lugli, F., Dong, X., Depalmas, A., Melis, R., Cipriani, A., Cheng, H., Zanchetta, G., and De Waele, J.: Speleothems uncover Late Holocene environmental changes across the Nuragic period in Sardinia (Italy):

https://doi.org/10.5194/egusphere-2026-4435
Preprint. Discussion started: 7 August 2026

A possible human influence on land use during Bronze to post-Iron Age cultural shifts, *Quat. Sci. Rev.*, 328, 108542, https://doi.org/10.1016/j.quascirev.2024.108542, 2024.

Columbu, A., Isola, I., Zanchetta, G., Drysdale, R. N., Natali, S., Hellstrom, J. C., Fallick, A. E., and co-authors: Speleothem evidence of late glacial and Early Holocene Preboreal and Boreal hydro-climate changes in the western Mediterranean (Corchia Cave, Italy), *Quat. Sci. Rev.*, 354, 109241, https://doi.org/10.1016/j.quascirev.2025.109241, 2025.

Comas-Bru, L., Harrison, S. P., Werner, M., Rehfeld, K., Scroxton, N., Veiga-Pires, C., and SISAL Working Group Members: Evaluating model outputs using integrated global speleothem records of climate change since the last glacial, *Clim. Past,* 15, 1557–1579, https://doi.org/10.5194/cp-15-1557-2019, 2019.

de Graaf, S., Vonhof, H. B., Levy, E. J., Markowska, M., Haug, G. H., and Meckler, A. N.: A comparison of isotope ratio mass spectrometry and cavity ring-down spectroscopy techniques for isotope analysis of fluid inclusion water*, Rapid Commun. Mass Spectrom.,* 34, e8837, https://doi.org/10.1002/rcm.8837, 2020.

Deininger, M., Hansen, M., Fohlmeister, J., Schröder-Ritzrau, A., Burstyn, Y., and Scholz, D.: Are oxygen isotope fractionation factors between calcite and water derived from speleothems systematically biased due to prior calcite precipitation (PCP)?, *Geochim. Cosmochim. Acta,* 305, 212–227, https://doi.org/10.1016/j.gca.2021.03.026, 2021.

Demény, A., Rinyu, L., Kern, Z., Hatvani, I. G., Czuppon, G., Surányi, G., Leél-Őssy, S., Shen, C.-C., and Koltai, G.: Paleotemperature reconstructions using speleothem fluid inclusion analyses from Hungary, *Chem. Geol.,* 563, 120038, https://doi.org/10.1016/j.chemgeo.2020.120038, 2021.

deMenocal, P. B., Ortiz, J., Guilderson, T., Adkins, J., Sarnthein, M., Baker, L., and Yarusinsky, M.: Abrupt onset and termination of the African Humid Period: Rapid climatic responses to gradual insolation forcing, *Quat. Sci. Rev.,* 19, 347–361, https://doi.org/10.1016/S0277-3791(99)00081-5, 2000.

Fairchild, I. J. and McMillan, E. A.: Speleothems as indicators of wet and dry periods, *Int. J. Speleol.,* 36, 69–74, https://doi.org/10.5038/1827-806X.36.2.2, 2007.

Fairchild, I. J., Smith, C. L., Baker, A., Fuller, L., Spötl, C., Mattey, D., and McDermott, F.: Modification and preservation of environmental signals in speleothems, *Earth-Sci. Rev.,* 75, 105–153, https://doi.org/10.1016/j.earscirev.2005.08.003, 2006.

Fernandez, A., Løland, M. H., Maccali, J., Krüger, Y., Vonhof, H. B., Sodemann, H., and Meckler, A. N.: Characterization and correction of evaporative artifacts in speleothem fluid inclusion isotope analyses as applied to a stalagmite from Borneo, *Geochem. Geophys. Geosyst.,* 24, e2023GC010857, https://doi.org/10.1029/2023GC010857, 2023.

Frisia, S.: Microstratigraphic logging of calcite fabrics in speleothems as tool for palaeoclimate studies, *Int. J. Speleol.,* 44, 1–16, https://doi.org/10.5038/1827-806X.44.1.1, 2015.

García-Alix, A., Jiménez-Moreno, G., Jiménez-Espejo, F. J., Anderson, R. S., and Delgado-Huertas, A.: Paleohydrological dynamics in the western Mediterranean during the last glacial cycle, *Glob. Planet. Change*, 197, 103391, https://doi.org/10.1016/j.gloplacha.2020.103391, 2021.

García-Alix, A., Jiménez-Moreno, G., Gázquez, F., Monedero-Contreras, R., López-Avilés, A., Jiménez-Espejo, F. J., Rodríguez-Rodríguez, M., Camuera, J., Ramos-Román, M. J., and Anderson, R. S.: Climatic control on the Holocene hydrology of a playa-lake system in the western Mediterranean, *Catena*, 214, 106292, https://doi.org/10.1016/j.catena.2022.106292, 2022.

García-López, S.; Vélez-Nicolás, M.; Salazar-Rojas, M.; Ruiz-Ortiz, V.; Sánchez-Bellón, Á., Gómez-Hernández, J. J., and other co-authors: Isotopic and remote sensing-based characterisation of a rainfall event over western Sierra de Gádor (Spain): Implications for carbonate aquifer recharge, *Water*, 15, 4252, https://doi.org/10.3390/w15244252, 2023.

Gázquez, F., Calaforra, J. M., Evans, N. P., and Hodell, D. A.: Using stable isotopes ($\delta^{17}O$, $\delta^{18}O$ and δD) of gypsum hydration water to ascertain the role of water condensation in the formation of subaerial gypsum speleothems, *Chem. Geol.,* 452, 34–46, https://doi.org/10.1016/j.chemgeo.2017.01.028, 2017.

Gázquez, F., Voigt, C., Castillo-Baquera, A., García-Alix, A., Jiménez-Moreno, G., Jiménez-Espejo, F. J., and co-authors: Quantifying atmospheric humidity in the western Mediterranean during the Iron Age and the Roman Era, *Geophys. Res. Lett.,* 52, e2025GL120424, https://doi.org/10.1029/2025GL120424, 2025.

Genty, D., Plagnes, V., Causse, C., Cattani, O., Stiévenard, M., Falourd, S., Blamart, D., Ouahdi, R., and Van-Exter, S.: Fossil water in large stalagmite voids as a tool for paleoprecipitation stable isotope composition reconstitution and paleotemperature calculation, *Chem. Geol.*, 184, 83–95, https://doi.org/10.1016/S0009-2541(01)00380-9, 2002.

Giménez, R., Bartolomé, M., Gázquez, F., Iglesias, M., and Moreno, A.: Underlying climate controls in triple oxygen (^{16}O, ^{17}O, ^{18}O) and hydrogen (^{1}H, ^{2}H) isotope composition of rainfall (Central Pyrenees), *Front. Earth Sci.*, 9, 633698, https://doi.org/10.3389/feart.2021.633698, 2021.

Giménez Luque, E. and Gómez Mercado, F.: Análisis de la flora vascular de la Sierra de Gádor (Almería, España), *Lazaroa*, 23, 35–43, 2002.

Griffiths, M. L., Drysdale, R. N., Vonhof, H. B., Gagan, M. K., Zhao, J.-X., Ayliffe, L. K., Hantoro, W. S., Hellstrom, J. C., Cartwright, I., Frisia, S., and Suwargadi, B. W.: Younger Dryas–Holocene temperature and rainfall history of southern Indonesia from $\delta^{18}O$ in speleothem calcite and fluid inclusions, *Earth Planet. Sci. Lett.*, 295, 30–36, https://doi.org/10.1016/j.epsl.2010.03.036, 2010.

Heiri, O., Ilyashuk, B., Millet, L., Samartin, S., and Lotter, A. F.: Stacking of discontinuous regional palaeoclimatic records: Chironomid-based summer temperatures from the Alpine region, *Holocene*, 25, 137–149, https://doi.org/10.1177/0959683614556382, 2015.

Jiménez-Moreno, G. and Anderson, R. S.: Holocene vegetation and climate change recorded in alpine bog sediments from the Borreguiles de la Virgen, Sierra Nevada, southern Spain, *Quat. Res.,* 77, 44–53, https://doi.org/10.1016/j.yqres.2011.09.006, 2012.

Jiménez-Espejo, F. J., García-Alix, A., Jiménez-Moreno, G., Rodrigo-Gámiz, M., Anderson, R. S., Rodríguez-Tovar, F. J., and Pardo-Igúzquiza, E.: Saharan aeolian input and effective humidity variations over western Europe during the Holocene from a high-altitude record, *Chem. Geol.,* 374–375, 1–12, https://doi.org/10.1016/j.chemgeo.2014.03.001, 2014.

https://doi.org/10.5194/egusphere-2026-4435
Preprint. Discussion started: 7 August 2026

Jiménez-Moreno, G., García-Alix, A., Anderson, R. S., Ramos-Román, M. J., Camuera, J., Mesa-Fernández, J. M., Jiménez-Espejo, F. J., López-Avilés, A., Rodrigo-Gámiz, M., and López-Blanco, C.: Late Pleistocene and Holocene environmental and climate reconstruction from Sierra Nevada, Spain, *Limnetica*, 45, https://doi.org/10.23818/limn.45.22, 2026.

Jiménez-Moreno, G., Prat, N., Heiri, O., García-Alix, A., Anderson, R. S., Jiménez-Espejo, F. J., Camuera, J., and López-Blanco, C.: Chironomid-based Holocene summer temperature dynamics from southern Spain, *Quat. Sci. Rev.,* 369, 109647, https://doi.org/10.1016/j.quascirev.2025.109647, 2025.

Jiménez-Moreno, G., Heiri, O., García-Alix, A., Anderson, R. S., Jiménez-Espejo, F. J., López-Blanco, C., Jiménez, L., Pérez-Martínez, C., Rodrigo-Gámiz, M., López-Avilés, A., and Camuera, J.: Holocene summer temperature reconstruction based on a chironomid record from Sierra Nevada, southern Spain, *Quat. Sci. Rev.,* 319, 108343, https://doi.org/10.1016/j.quascirev.2023.108343, 2023.

Levy, E. J., Vonhof, H. B., Bar-Matthews, M., Martínez-García, A., Ayalon, A., Matthews, A., Silverman, V., Raveh-Rubin, S., Zilberman, T., Yasur, G., Schmitt, M., and Haug, G. H.: Weakened AMOC related to cooling and atmospheric circulation shifts in the last interglacial eastern Mediterranean, *Nat. Commun.,* 14, 5180, https://doi.org/10.1038/s41467-023-40880-z, 2023.

López-Elorza, M., Muñoz-García, M. B., González-Acebrón, L., and Martín-Chivelet, J.: Fluid-inclusion petrography in calcite stalagmites: Implications for entrapment processes, *J. Sediment. Res.,* 91, 1206–1226, https://doi.org/10.2110/jsr.2021.016, 2021.

Luppichini, M., Natali, S., Columbu, A., and Bini, M.: Mediterranean precipitation variability is driven by complex atmospheric mechanisms beyond the North Atlantic Oscillation, *Commun. Earth Environ*., https://doi.org/10.1038/s43247-025-02420-9, 2025.

Markowska, M., Cuthbert, M. O., Baker, A., Treble, P. C., Andersen, M. S., Adler, L., Griffiths, A., and Frisia, S.: Modern speleothem oxygen isotope hydroclimate records in water-limited SE Australia, *Geochim. Cosmochim. Acta*, 270, 431–448, https://doi.org/10.1016/j.gca.2019.12.007, 2020.

Mayoral, J., Barranco, P., and Fernández-Cortés, A.: First biological data, associated fauna, and microclimate preferences of the enigmatic cave-dwelling beetle *Dalyat mirabilis* Mateu, 2002 (Coleoptera, Carabidae), *Subterr. Biol.*, 44, 103–121, https://doi.org/10.3897/subtbiol.44.87205, 2022.

Moreno, A., Pérez-Mejías, C., Bartolomé, M., Sancho, C., Cacho, I., Stoll, H., Delgado-Huertas, A., Hellstrom, J., Edwards, R. L., and Cheng, H.: New speleothem data from Molinos and Ejulve caves reveal Holocene hydrological variability in northeast Iberia, *Quat. Res.*, 88, 223–233, https://doi.org/10.1017/qua.2017.45, 2017.

Paredes, D., Trigo, R. M., Garcia-Herrera, R., and Trigo, I. F.: Understanding precipitation changes in Iberia in early spring: Weather typing and storm-tracking approaches, *J. Hydrometeorol.*, 7, 101–113, https://doi.org/10.1175/JHM472.1, 2006.

Parker, S. E., Harrison, S. P., Comas-Bru, L., Kaushal, N., LeGrande, A. N., and Werner, M.: A data–model approach to interpreting speleothem oxygen isotope records from monsoon regions, *Clim. Past*, 17, 1119–1138, https://doi.org/10.5194/cp-17-1119-2021, 2021.

https://doi.org/10.5194/egusphere-2026-4435
Preprint. Discussion started: 7 August 2026

Patterson, E. W., Skiba, V., Wolf, A., Griffiths, M. L., McGee, D., Bùi, T. N., Trần, M. X., Đinh, T. H., Đỗ-Trọng, Q., Goldsmith, G. R., Ersek, V., and Johnson, K. R.: Local hydroclimate alters interpretation of speleothem $\delta^{18}O$ records, *Nat. Commun.*, 15, 9064, https://doi.org/10.1038/s41467-024-53422-y, 2024.

Pérez-Mejías, C., Wang, J., Ning, Y., Moreno, A., Delgado-Huertas, A., Edwards, R. L., Cheng, H., and Stoll, H. M.: Climate controls on speleothem initial $^{234}U/^{238}U$ ratios in midlatitude settings over two glacial cycles, *Geochim. Cosmochim. Acta*, 389, 265–279, https://doi.org/10.1016/j.gca.2025.02.012, 2025.

Pérez-Mejías, C., Bernal-Wormull, J. L., Cheng, H., and Stoll, H. M.: Prior calcite precipitation systematics in stalagmites with detrital inputs, *Geochim. Cosmochim. Acta*, 419, 205–224, https://doi.org/10.1016/j.gca.2026.03.021, 2026.

Pulido-Bosch, A., Pulido-Leboeuf, P., Molina-Sánchez, L., Vallejos, A., and Martín-Rosales, W.: Intensive agriculture, wetlands, quarries and water management: A case study (Campo de Dalías, SE Spain), *Environ. Geol.,* 40, 163–168, https://doi.org/10.1007/s002540000160, 2000.

Ramos-Román, M. J., Jiménez-Moreno, G., Camuera, J., García-Alix, A., Anderson, R. S., Jiménez-Espejo, F. J., and Carrión, J. S.: Holocene climate aridification trend and human impact interrupted by millennial- and centennial-scale climate fluctuations from a new sedimentary record from Padul (Sierra Nevada, southern Iberian Peninsula), *Clim. Past,* 14, 117–137, https://doi.org/10.5194/cp-14-117-2018, 2018.

Rodrigo-Gámiz, M., Martínez-Ruiz, F., Rampen, S. W., Schouten, S., and Sinninghe Damsté, J. S.: Sea surface temperature variations in the western Mediterranean Sea over the last 20 kyr: A dual-organic proxy (U^{K}_{37} and LDI) approach, *Paleoceanography*, 29, 87–98, https://doi.org/10.1002/2013PA002466, 2014.

Rossi, C., Bajo, P., Lozano, R. P., and Hellstrom, J.: Younger Dryas to Early Holocene paleoclimate in Cantabria (N Spain): Constraints from speleothem Mg, annual fluorescence banding and stable isotope records, *Quat. Sci. Rev.,* 192, 71–85, https://doi.org/10.1016/j.quascirev.2018.05.025, 2018.

Ruíz-Caballero, E., Gázquez, F., Fernández-Cortés, A., Calaforra, J.M. Seasonal ventilation patterns in Larga Cave (Sierra de los Filabres, Almería, SE Spain), *Geogaceta*, 76, 67-70, https://doi.org/10.55407/geogaceta104506, 2024.

Sánchez-Martos, F., Torres Palenzuela, A., and García-Sánchez, J.: Avance de catálogo de cavidades del término municipal de Dalías (Sierra de Gádor, Almería), *Espeleotemas*, 1, 36–39, 1991.

Schröder, T., van't Hoff, J., López-Sáez, J. A., Viehberg, F., Melles, M., and Reicherter, K.: Holocene climatic and environmental evolution on the southwestern Iberian Peninsula: A high-resolution multi-proxy study from Lake Medina (Cádiz, SW Spain), *Quat. Sci. Rev.,* 198, 208–225, https://doi.org/10.1016/j.quascirev.2018.08.030, 2018.

Sha, L., Ait Brahim, Y., Wassenburg, J. A., Yin, J., Peros, M., Cruz, F. W., Cai, Y., Li, H., Du, W., Zhang, H., Edwards, R. L., and Cheng, H.: How far north did the African monsoon fringe expand during the African Humid Period? Insights from southwest Moroccan speleothems, *Geophys. Res. Lett.,* 46, 14093–14102, https://doi.org/10.1029/2019GL084879, 2019.

Spötl, C.: Long-term performance of the GasBench isotope ratio mass spectrometry system for the stable isotope analysis of carbonate microsamples, *Rapid Commun. Mass Spectrom*., 25, 1683–1685, https://doi.org/10.1002/rcm.5037, 2011.

Stachnik, A., Gázquez, F., Morales-González, A. L., González-Ramón, A., Moral-Martos, F., Jiménez-Espinosa, R., Morellón, M., and Chivelet, J.: A machine learning approach to assess the influence of atmospheric synoptic patterns (NAO vs. WeMO) on the isotopic composition of rainfall in southeastern Iberia, Egusphere preprint. https://doi.org/10.5194/egusphere-2026-2058, 2016.

Thatcher, D. L., Wanamaker, A. D., Denniston, R. D., Asmerom, Y., Polyak, V., Fullick, D., Ummenhofer, C. C., Gillikin, D. P., and Haws, J.: Hydroclimate variability from western Iberia (Portugal) during the Holocene: Insights from a composite stalagmite isotope record, *Holocene*, 30, 966–981, https://doi.org/10.1177/0959683620908648, 2020.

Toney, J. L., García-Alix, A., Jiménez-Moreno, G., Anderson, R. S., Moossen, H., and Seki, O.: New insights into Holocene hydrology and temperature from lipid biomarkers in western Mediterranean alpine wetlands, *Quat. Sci. Rev.*, 240, 106395, https://doi.org/10.1016/j.quascirev.2020.106395, 2020.

Torres, A.: IV Campamento Provincial Dalías'93, *Espeleotemas*, 4, 79–82, 1994.

Vallejos, A., Pulido-Bosch, A., Martín-Rosales, W., and Calvache, M. L.: Contribution of environmental isotopes to the understanding of complex hydrologic systems: A case study from Sierra de Gádor, SE Spain, *Earth Surf. Process. Landf.,* 22, 1157–1168, https://doi.org/10.1002/(SICI)1096-9837(199712)22:12<1157::AID-ESP816>3.0.CO;2-R, 1997.

Vandenschrick, G., van Wesemael, B., Frot, E., Pulido-Bosch, A., Molina, L., Stiévenard, M., and Souchez, R.: Using stable isotope analysis ($\delta^{18}O$) to characterise the regional hydrology of the Sierra de Gádor, SE Spain, *J. Hydrol.*, 265, 43–55, https://doi.org/10.1016/S0022-1694(02)00097-5, 2002.

Walczak, I. W., Baldini, J. U. L., Baldini, L. M., McDermott, F., Marsden, S., Standish, C. D., Richards, D. A., Andreo, B., and Slater, J.: Reconstructing high-resolution climate using CT scanning of unsectioned stalagmites: A case study identifying the mid-Holocene onset of the Mediterranean climate in southern Iberia, *Quat. Sci. Rev.,* 127, 117–128, https://doi.org/10.1016/j.quascirev.2015.09.010, 2015.

Warken, S. F., Weißbach, T., Kluge, T., Vonhof, H., Scholz, D., Vieten, R., Schmidt, M., Winter, A., and Frank, N.: Last glacial millennial-scale hydro-climate and temperature changes in Puerto Rico constrained by speleothem fluid inclusion $\delta^{18}O$ and $\delta^{2}H$ values, *Clim. Past,* 18, 167–188, https://doi.org/10.5194/cp-18-167-2022, 2022.

Wassenburg, J. A., Dietrich, S., Fietzke, J., Fohlmeister, J., Jochum, K. P., Scholz, D., Richter, D. K., Sabaoui, A., Spötl, C., Lohmann, G., Andreae, M. O., and Immenhauser, A.: Reorganization of the North Atlantic Oscillation during early Holocene deglaciation, *Nat. Geosci.,* 9, 602–605, https://doi.org/10.1038/ngeo2767, 2016.

Wassenburg, J. A., Vonhof, H. B., Cheng, H., Martínez-García, A., Ebner, P.-R., Li, X., Zhang, H., Sha, L., Tian, Y., Edwards, R. L., Fiebig, J., and Haug, G. H.: Penultimate deglaciation Asian monsoon response to North Atlantic circulation collapse, *Nat. Geosci.,* 14, 937–941, https://doi.org/10.1038/s41561-021-00851-9, 2021.